



# Spinal Cord Injury Changes the Structure and Functional Potential of Gut Bacterial and Viral Communities

Jingjie Du,<sup>a</sup> Ahmed A. Zayed,<sup>a,h</sup>  Kristina A. Kigerl,<sup>b,c,d,h</sup> Kylie Zane,<sup>e</sup> Matthew B. Sullivan,<sup>a,f,g,h</sup>  Phillip G. Popovich<sup>b,c,d,h</sup>

<sup>a</sup>Department of Microbiology, The Ohio State University, Columbus, Ohio, USA

<sup>b</sup>Department of Neuroscience, The Ohio State University College of Medicine, Columbus, Ohio, USA

<sup>c</sup>The Belford Center for Spinal Cord Injury, The Ohio State University College of Medicine, Columbus, Ohio, USA

<sup>d</sup>The Center for Brain and Spinal Cord Repair, The Ohio State University College of Medicine, Columbus, Ohio, USA

<sup>e</sup>Medical Scientist Training Program, The Ohio State University College of Medicine, Columbus, Ohio, USA

<sup>f</sup>Department of Civil, Environmental and Geodetic Engineering, The Ohio State University, Columbus, Ohio, USA

<sup>g</sup>Infectious Disease Institute, The Ohio State University, Columbus, Ohio, USA

<sup>h</sup>Center of Microbiome Science, The Ohio State University, Columbus, Ohio, USA

Jingjie Du, Ahmed A. Zayed, Kristina A. Kigerl, and Kylie Zane contributed equally to this article. Author order was determined based on relative contribution to design and execution of experimental methodology, writing/revision/editing, and visualization of experimental data.

**ABSTRACT** Emerging data indicate that gut dysbiosis contributes to many human diseases, including several comorbidities that develop after traumatic spinal cord injury (SCI). To date, all analyses of SCI-induced gut dysbiosis have used 16S rRNA amplicon sequencing. This technique has several limitations, including being susceptible to taxonomic “blind spots,” primer bias, and an inability to profile microbiota functions or identify viruses. Here, SCI-induced gut dysbiosis was assessed by applying genome- and gene-resolved metagenomic analysis of murine stool samples collected 21 days after an experimental SCI at the 4th thoracic spine (T4) or 10th thoracic spine (T10) spinal level. These distinct injuries partially (T10) or completely (T4) abolish sympathetic tone in the gut. Among bacteria, 105 medium- to high-quality metagenome-assembled genomes (MAGs) were recovered, with most ( $n=96$ ) representing new bacterial species. Read mapping revealed that after SCI, the relative abundance of beneficial commensals (*Lactobacillus johnsonii* and *CAG-1031* spp.) decreased, while potentially pathogenic bacteria (*Weissella cibaria*, *Lactococcus lactis\_A*, *Bacteroides thetaiotaomicron*) increased. Functionally, microbial genes encoding proteins for tryptophan, vitamin B<sub>6</sub>, and folate biosynthesis, essential pathways for central nervous system function, were reduced after SCI. Among viruses, 1,028 mostly novel viral populations were recovered, expanding known murine gut viral species sequence space ~3-fold compared to that of public databases. Phages of beneficial commensal hosts (*CAG-1031*, *Lactobacillus*, and *Turicibacter*) decreased, while phages of pathogenic hosts (*Weissella*, *Lactococcus*, and class *Clostridia*) increased after SCI. Although the microbiomes and viromes were changed in all SCI mice, some of these changes varied as a function of spinal injury level, implicating loss of sympathetic tone as a mechanism underlying gut dysbiosis.


**IMPORTANCE** To our knowledge, this is the first article to apply metagenomics to characterize changes in gut microbial population dynamics caused by a clinically relevant model of central nervous system (CNS) trauma. It also utilizes the most current approaches in genome-resolved metagenomics and viromics to maximize the biological inferences that can be made from these data. Overall, this article highlights the importance of autonomic nervous system regulation of a distal organ (gut) and its microbiome inhabitants after traumatic spinal cord injury (SCI). By providing information on taxonomy, function, and viruses, metagenomic data may better

**Citation** Du J, Zayed AA, Kigerl KA, Zane K, Sullivan MB, Popovich PG. 2021. Spinal cord injury changes the structure and functional potential of gut bacterial and viral communities. *mSystems* 6:e01356-20. <https://doi.org/10.1128/mSystems.01356-20>.

**Editor** Mani Arumugam, University of Copenhagen

**Copyright** © 2021 Du et al. This is an open-access article distributed under the terms of the [Creative Commons Attribution 4.0 International license](https://creativecommons.org/licenses/by/4.0/).

Address correspondence to Matthew B. Sullivan, [sullivan.948@osu.edu](mailto:sullivan.948@osu.edu), or Phillip G. Popovich, [phillip.popovich@osumc.edu](mailto:phillip.popovich@osumc.edu).

 This is the first manuscript to apply metagenomics to characterize changes in gut microbial populations caused by SCI. Using genome-resolved metagenomics and viromics, we show the importance of SNS regulation of the gut and its microbiome after SCI.

**Received** 23 December 2020

**Accepted** 25 March 2021

**Published** 11 May 2021

predict how SCI-induced gut dysbiosis influences systemic and neurological outcomes after SCI.

**KEYWORDS** gut dysbiosis, metagenomics, microbiome, spinal cord injury, virome

Gut microbiota protect mammals from pathogen colonization (reviewed in reference 1), regulate gut permeability (2), stimulate the immune system (reviewed in reference 1), synthesize essential vitamins (reviewed in reference 3), produce secondary bile acids (4, 5), produce short-chain fatty acids (SCFAs), and provide metabolic fuel for colonocytes by breaking down indigestible food sources (6, 7). Gut microbes are also key components of the “brain-gut axis,” i.e., the bidirectional system of communication between the central nervous system (CNS) and the digestive system. Gut microbes have been shown to be essential for normal CNS development, functioning, and recovery after injury (8–11) and for regulating host neural activity and behavior in response to environmental cues (12). Indeed, gut-derived microbes produce various neuroactive metabolites or precursor molecules (e.g., tryptophan), which are needed to synthesize serotonin, dopamine, gamma-aminobutyric acid (GABA), acetylcholine, and melatonin (13). These neuroactive metabolites signal the CNS via vagal afferents, or they enter the circulation and pass directly into the neural parenchyma across the blood-brain barrier (14, 15). Gut microbes are also capable of indirectly signaling the CNS by influencing innate and adaptive immunity; and the immune system, like the gut, exerts bidirectional communication with the CNS (reviewed in reference 16).

Homeostasis of the gastrointestinal (GI) tract, including microbial homeostasis, is dependent on the enteric nervous system of the GI tract, which is innervated by the parasympathetic efferents from the vagus nerve and sacral spinal cord, presympathetic nerves originating in the brainstem, and sympathetic efferents originating exclusively from the spinal cord (17, 18). When the spinal cord is injured, axons that normally descend from the brain/brainstem to control spinal sympathetic neurons are lost or damaged (17). Consequently, after spinal cord injury (SCI), normal sympathetic control of the small bowel and colon is lost, leading to impaired gut motility, mucosal secretions, vascular tone, and immune function (19). Loss or disruption of one or more of these GI functions after SCI can disrupt the ecological balance of microorganisms in the gut, causing dysbiosis (20, 21). Indeed, lasting changes in gut bacterial composition have been documented in multiple clinical and preclinical studies of SCI (22–27). Disruption of this gut microbial ecosystem has been linked to various comorbidities that develop after SCI, such as metabolic disease, immune dysfunction, and mental and cognitive impairment (28–31). Unfortunately, because all published reports of SCI-induced gut dysbiosis have used 16S rRNA amplicon sequencing to characterize compositional changes in gut bacteria, reliable predictions about microbiota function remain elusive, as do data describing SCI-induced compositional changes in novel microbial species, including viruses (21).

Because viruses lack universal marker genes for taxonomic assignment, the genetic diversity of the gut virome remains largely unknown (32, 33). As the most abundant members of the enteric virome (34), bacteriophages may affect human health and disease by dramatically shaping gut bacterial communities and their functions. This can occur through predator-prey dynamics (reviewed in reference 35) and horizontal gene transfer (36) or by direct interactions between viruses and the immune system (37–40), even including a phage-mediated, non-host-derived immunity to protect against invading pathogens (41). There may or may not be a “healthy gut virome” (34, 42–44), but it is clear that individuals have unique, persistent viromes (42, 43). In the context of disease, disease-specific virome changes have been observed for inflammatory bowel disease (IBD) (45), ulcerative colitis (46), autism spectrum disorders (ASD) (47), colorectal cancer (48), type 1 diabetes (49, 50), and type 2 diabetes (51). However, it is notable that rather than considering all taxa as is done in environmental studies (52–54), most gut virome studies have limited their analyses to known taxonomy or missed the

linkage of viruses to their hosts (55, 56). Nothing is yet known about how the gut virome is affected by SCI.

All forms of SCI examined to date cause gut dysbiosis (19, 22–27), but what remains unclear is whether SCI-induced changes in microbial population dynamics and the functional implications of those changes vary as a function of spinal injury level and/or injury severity. To expand upon current knowledge of SCI-induced gut dysbiosis, we use metagenomics to examine ecological and functional changes in gut bacterial and viral communities after SCI in a murine model, controlling for diet and antibiotic exposure (common confounders for microbiome studies) (22, 23, 57). Ecological and functional changes in the gut microbiota were compared in mice receiving SCI at the 4th thoracic spine (T4) or 10th thoracic spine (T10) spinal levels. We show that the severity of gut dysbiosis is affected by spinal injury level; more robust changes were noted when SCI occurred at high spinal levels (T4), which causes greater imbalance in autonomic tone in the gut. Our novel data also reveal SCI-dependent changes in the microbiome and virome, as well as related metabolic pathways, providing a myriad of new hypotheses to guide future SCI studies.

## RESULTS AND DISCUSSION

**The composition and magnitude of change in gut microbiota caused by SCI vary as a function of spinal injury level.** We hypothesized that sympathetic nervous system control over proximal and distal intestines will vary as a function of spinal injury level, causing differences in intestinal function that will directly affect the composition of the gut microbiome. The sympathetic preganglionic neurons (SPNs) controlling the small and large intestines are located primarily in the intermediolateral cell column in thoracic spinal segments T5 to T10 (58–60). Therefore, most brain and brainstem control over spinal autonomic networks that innervate the gut are lost when SCI occurs at or above the T5 spinal level. When SCI occurs at lower spinal levels, some reflex control over spinal autonomic neurons remains intact, with the magnitude of intact circuitry varying as a function of injury level and severity. To date, there have been no controlled studies to assess how the gut microbiota responds to SCI when there is some or no preservation of executive control (from brain/brainstem) over spinal autonomic reflexes, although data from human subject research predicts that spinal-level-dependent differences do exist. Indeed, the composition of gut microbiota in individuals with cervical SCI was found to be distinct from that in people with thoracic or lumbar SCI (23). Here, to directly test the hypothesis that the composition and magnitude of change in SCI-induced gut dysbiosis varies as a function of spinal injury level, three groups of mice were prepared ( $n = 15$  mice in total;  $n = 5$ /group). Sham-injured control mice underwent laminectomy surgery at vertebral level T4 without spinal cord injury (Lam controls). Mice in the remaining two groups received a severe crush injury of the spinal cord at either the T10 or T4 spinal level. Based on published data, these two distinct spinal injury levels either partially preserve (T10) or abolish (T4) sympathetic innervation of the gut (58–61). Because gut microbes are transferable among species that share the same habitat, all mice were singly housed throughout the study, starting 2 weeks before SCI. At 21 days postinjury (dpi), fecal samples were collected and then individually prepared for microbiome analysis (Fig. 1A). The 21-dpi time period was chosen because published data indicate that gut dysbiosis fully develops at this time postinjury (19).

To characterize microbial community composition in each group, microbial taxa were identified using read-based and assembly-based approaches (see Materials and Methods and Fig. S1 in the supplemental material). A set of 14 single-copy marker genes were directly detected from the metagenomic reads using Hidden Markov Model (HMM) profiles, allowing for higher taxonomic (strain-level) resolution than is achievable by 16S rRNA gene sequencing and also avoiding the copy number variation problem that limits abundance estimation in 16S rRNA gene sequencing (62). Abundance-based comparisons (principal-coordinate analysis [PCoA] of Bray-Curtis dissimilarities using ribosomal protein L2 [rplB]; see Materials and Methods) of all

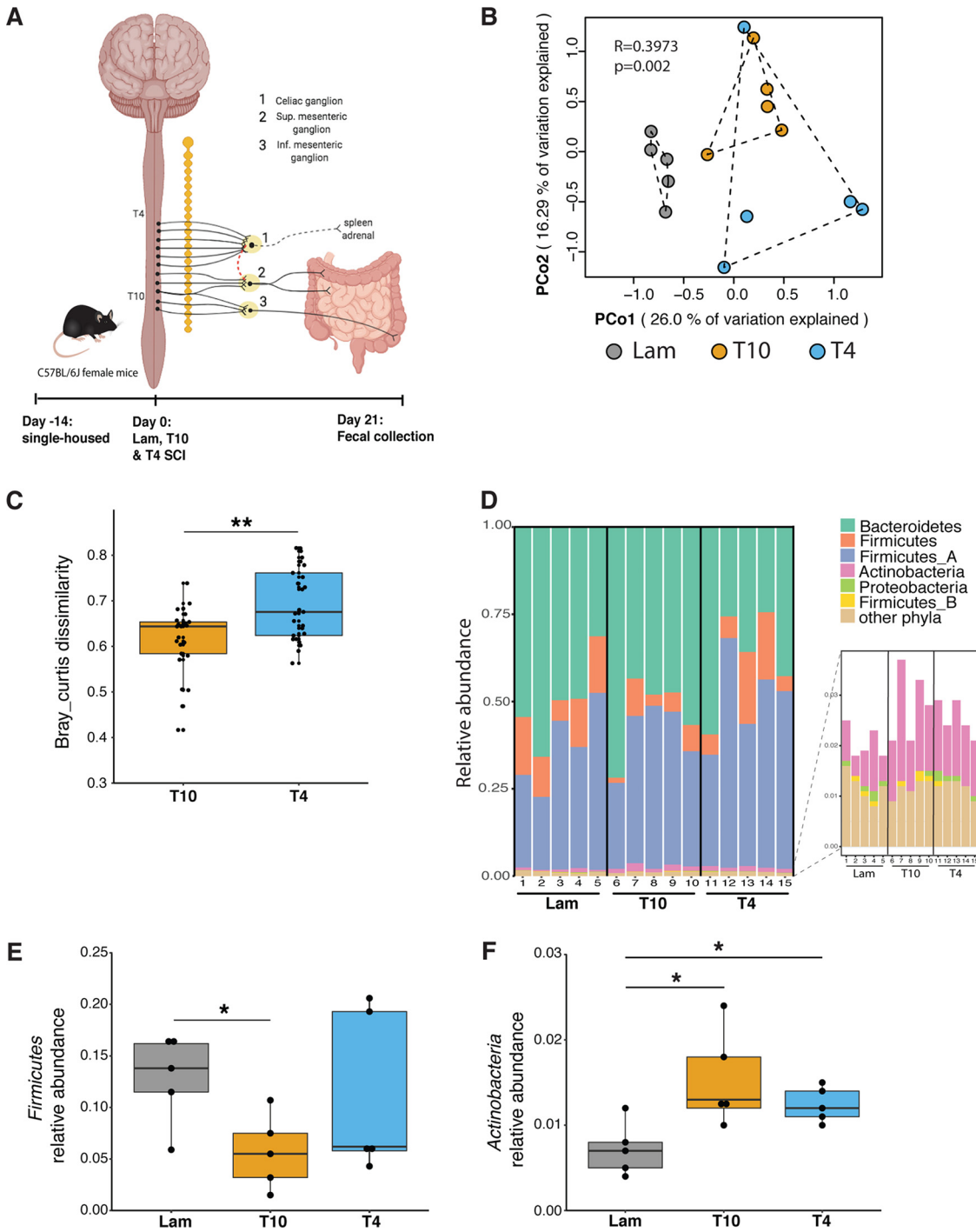


**FIG 1** Intestinal microbial community composition was disturbed after spinal cord injury. (A) Fifteen mice were equally divided among three treatment groups: a sham surgery control group (Lam), an SCI group modeling injury at vertebral level T10, and an SCI group modeling injury at vertebral level T4. At 21 days postinjury, one fecal sample per mouse was collected for bulk microbiome isolation. (B) Principal-coordinate analysis (PCoA) of Bray-Curtis distances shows that microbial communities are different between the Lam, T4, and T10 groups (PERMANOVA,  $R=0.3973$ ,  $P=0.002$ ). Each data point indicates an individual mouse sample. (C) Box plot analysis showing the Bray-Curtis dissimilarities between the control group (Lam) and T4 or T10 SCI microbial communities. Each data point represents one Bray-Curtis dissimilarity comparison between individual samples in each of the other groups (Lam versus T4/T10;  $n=5$  of one group were individually compared to  $n=5$  from another group for a total of 25 comparisons between the Lam and T4 or T10 groups, respectively). A higher score suggests a higher dissimilarity of different individuals between the Lam and SCI groups (T4/T10). \*\*,  $P<0.01$  by Wilcoxon rank sum test with a false discovery rate (FDR) of  $<0.05$  calculated by “*fd*” in R. (D) Intestinal microbial community composition at the phylum level. On the x axis, the numbers 1 to 15 represent individual mice within each group. (E and F) Box plots showing the relative abundance of the phyla *Firmicutes* (E) and *Actinobacteria* (F). All box plots shown display the median and quartiles, with each dot in the box plot representing an individual mouse sample, and each group (Lam, T4, T10) contains five samples. Read-based estimates of relative abundances of microbial taxa (see Materials and Methods) were used for all the analyses displayed. \*,  $P<0.05$  (by Wilcoxon rank sum test; FDR  $<0.05$ ).

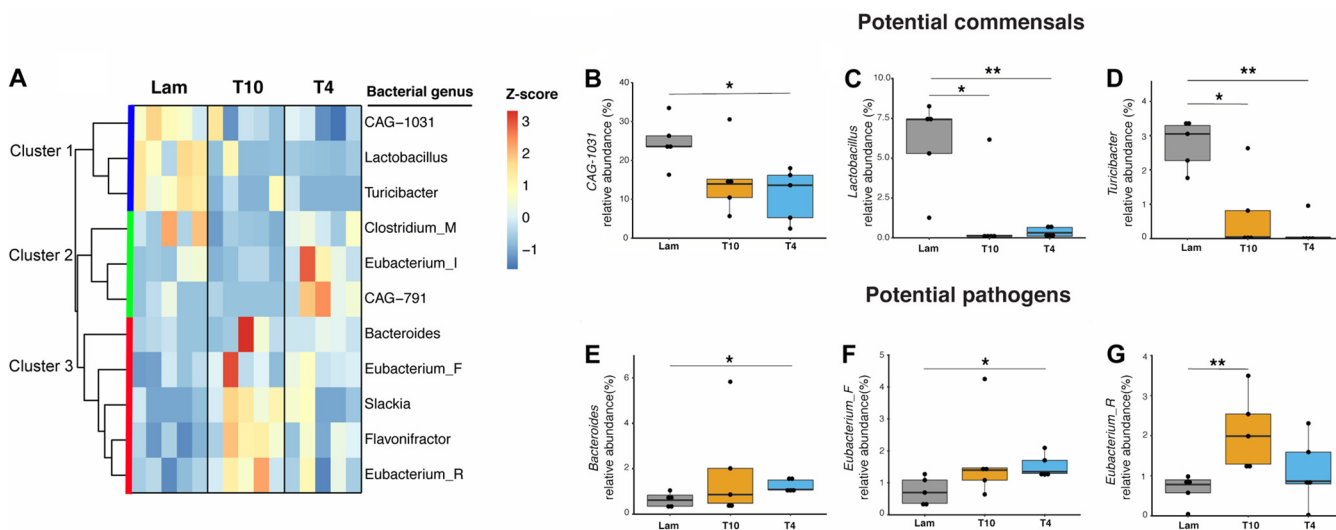


**FIG 2** Genus-level bacterial abundances are altered after SCI. (A) Hierarchical clustering of differentially abundant bacterial genera ( $P < 0.05$  by Wilcoxon rank sum test with a false discovery rate [FDR] of  $< 0.05$ ) shows three distinct clusters. Box plot analysis of select bacterial genera (with at least 0.5% relative abundance in any experimental group) indicates that *Lactobacillus*, *CAG-1031*, and *Turicibacter* (B to D) decreased after SCI, while *Bacteroides*, *Eubacterium\_F*, and *Eubacterium\_R* (E to G) increased after SCI in one injury level, compared to Lam controls. All box plots shown display the median and quartiles, with each dot in the box plot representing an individual mouse sample. Five individual mouse samples were used in each group. Read-based estimates of relative abundances of bacterial taxa (see Materials and Methods) were used for all the analyses displayed. \*\*,  $P < 0.01$ ; \*,  $P < 0.05$  (by Wilcoxon rank sum test). Analyses were done with an FDR of  $< 0.05$ .

microbial taxa present within the microbiome of each mouse revealed that the SCI groups cluster separately from those of Lam controls (permutational multivariate analysis of variance [PERMANOVA]  $R = 0.3973$ ,  $P = 0.002$ ), indicating that SCI, regardless of injury level, disrupts microbial community structure (Fig. 1B). When we compared the between-group Bray-Curtis dissimilarity of each SCI group (T4 or T10) to healthy controls (Lam), we found that gut dysbiosis is exacerbated in mice with high-level T4 SCI (Fig. 1C). While 27.6% of the microbial operational taxonomic units (OTUs) (clustered at 97% nucleotide identity using the ribosomal protein L2) were shared between the different experimental groups (Fig. S2A), most (81.3%) of the unshared OTUs were rare species ( $< 0.01\%$  relative abundance), which limits how confidently we can ascribe their presence/absence (Data Set S1, tab 1). There was no difference in Shannon's  $H$  between treatments (Fig. S2B).

Focusing in from the overall community comparisons, we next looked at changes that occurred at the phylum level. Among comparisons of 6 phyla ( $> 0.1\%$  relative abundance), the relative abundances of only two phyla changed significantly. By following the most recent Genome Taxonomy Database (GTDB) classification (63) (see Materials and Methods), these phyla were the *Firmicutes*, which was less abundant in the T10 SCI group (Fig. 1D and E), and the *Actinobacteria*, which was more abundant in both T10 and T4 SCI groups (Fig. 1D and F) than in our control group. We note that GTDB taxonomy separates the *Firmicutes*, *Firmicutes\_A*, and *Firmicutes\_B* into three separate phyla, which may be confusing but is phylogenomically well supported. Increased *Actinobacteria* may be associated with intestinal inflammation after SCI, as it has been in other inflammatory conditions like IBD (64), obesity (65), and rheumatoid arthritis (RA) (66).

While relatively few phyla changed significantly between groups, there were many more changes at the genus level: 11 bacterial genera were differentially abundant (Wilcoxon rank sum test,  $P < 0.05$ , false discovery rate [FDR]  $< 0.05$ ) (Data Set S1, tab 2) between control and SCI groups (Fig. S2C, red text). Hierarchical clustering of these 11 bacterial genera identified three distinct clusters (Fig. 2A). Cluster 1 comprised genera that were less abundant in both SCI groups than in the Lam controls. Clusters 2 and 3 were composed of genera that had greater abundance in the T4 and T10 SCI groups, respectively, highlighting injury level-dependent effects on a subset of genera. Of

these, one highly abundant taxon (>20% relative abundances in Lam), *CAG-1031*, was consistently less abundant in the T4 SCI group (Wilcoxon rank sum test,  $P < 0.05$ ,  $FDR < 0.05$ ) (Fig. 2B). Two other abundant taxa (>1% relative abundance in Lam), *Lactobacillus* and *Turicibacter*, were less abundant in the T4 or T10 SCI groups (Wilcoxon rank sum test,  $P < 0.05$ ,  $FDR < 0.05$ ) (Fig. 2C and D). *Turicibacter* spp. have been shown to promote host serotonin biosynthesis (67), while members of the *Lactobacillus* and *CAG-1031* genera are involved in key metabolic transformations in the gut (discussed below). A decrease in abundant commensals and probiotics also could open niches for antagonistic commensals and pathobionts. Notably, seven taxa were more abundant in the T10 (*Eubacterium\_R* and *Lachnospira*) or T4 (*Bacteroides*, *Weissella*, *Eubacterium\_F*, *UBA9475*, and *Neglecta*) SCI groups than in controls (Fig. 2E to G; Fig. S2D). Most of these taxa, *Eubacterium\_R*, *Lachnospira*, *Eubacterium\_F*, *UBA9475*, and *Neglecta*, fall within the class *Clostridia* (Fig. 2F and G). Previously, using 16S RNA gene sequencing, we found that the *Clostridiales*, members of the class *Clostridia*, increase after SCI and that their relative abundance inversely correlated with recovery of motor function, suggesting that these microbes may adversely affect neurological function (19, 68).

Collectively, the above data suggest that gut dysbiosis is a consistent phenomenon after SCI but that greater disruption of sympathetic control over the colon, such as after high-level (T4) SCI, may drive distinct changes in the gut microbiota.

**Genome-centric view of SCI-induced changes of gut microbiota.** The above read-based analyses rely upon mapping to single-copy marker genes. At the community level, read-based analysis provides information for any microbes that have reference genomes available, and so read-based analyses are best used for assessing diversity patterns. However, metagenome-assembled genomes (MAGs) provide population genomes for the specific variants occurring in these samples as well as lineage-specific pathway- and gene-level information that can then be used to develop novel hypotheses regarding the functional capabilities and ecological niches for these microbes. Therefore, to further assess changing taxonomic patterns and infer microbial functions, we assembled the shotgun sequence data from each sample and then binned contigs to create *de novo* draft microbial genomes, i.e., MAGs. MAGs enable robust, genome-informed taxonomic classification within a sample and rather than predicting function from slow-evolving taxonomic marker genes, MAGs provide maps of ecologically relevant functional potential for known taxa (69). Using this approach, we recovered 112 MAGs (>60% complete, <10% contamination), including 105 MAGs of medium ( $n = 35$ ; >70% complete, <10% contamination) to high ( $n = 70$ ; >90% complete, <5% contamination) quality (see Materials and Methods) that recruited, on average, 54.7% of the quality-controlled sequencing reads (Data Set S1, tab 3). Most ( $n = 96$ ) of these 105 MAGs represent previously unknown bacterial species as assessed against the GTDB-Tk v0.1.3 (63), the largest curated genomic taxonomy database available (69) (see Materials and Methods; Data Set S1, tab 4). Across the data set, 25 MAGs were differentially abundant between the Lam and SCI groups (Wilcoxon rank sum test,  $P < 0.05$ ,  $FDR < 0.05$ ) (Fig. 3A; Fig. S3 and Data Set S1, tab 5).

Similar to what our analysis with single-copy marker genes showed at the genus level, hierarchical clustering of the 25 differentially abundant MAGs revealed 3 distinct clusters (Fig. 3A). Cluster 1 identifies bacterial species that were less abundant in SCI groups than in Lam controls, regardless of injury level. Cluster 2 species were of greater abundance only in the T4 high-level SCI group, and cluster 3 species were of greater abundance in both T4 and T10 SCI groups (Fig. 3A). These data again show that there are both injury-level-dependent and -independent changes in gut microbiota after SCI. Only one previously known species, *Lactobacillus johnsonii*, was significantly less abundant after both T4 and T10 SCI (Wilcoxon rank sum test,  $P < 0.05$ ,  $FDR < 0.05$ ) (Fig. 3B). This species has widely been considered beneficial due to its anti-inflammatory effects (70–73) and its ability to metabolize inulin into a prebiotic that is further metabolized to short-chain fatty acids (SCFAs) like butyrate and propionate (74–77). Analysis of our

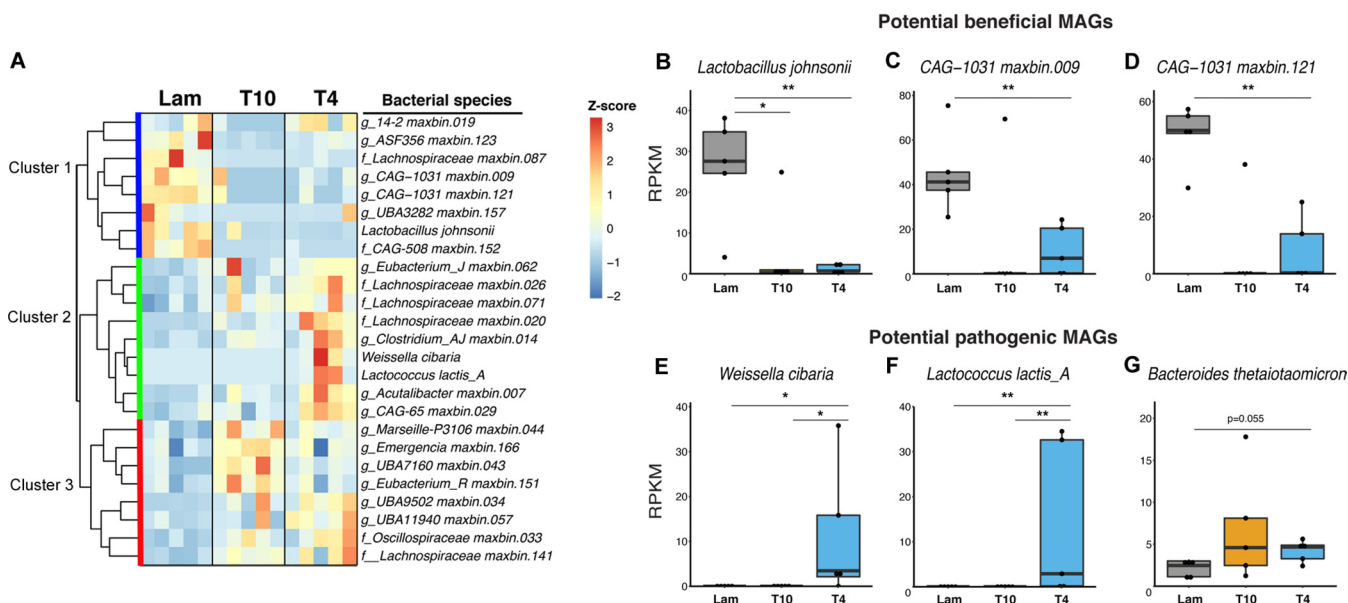


**FIG 3** Species-level bacterial abundances are altered after SCI. (A) Hierarchical clustering of differentially abundant bacterial species ( $P < 0.05$  by Wilcoxon rank sum test with a false discovery rate [FDR] of  $< 0.05$ ) shows three distinct clusters. Box plot analysis of select bacterial species shows that *Lactobacillus johnsonii* and two *CAG-1031* MAGs decreased after SCI (B to D), while *Weissella cibaria*, *Lactococcus lactis\_A*, and *Bacteroides thetaiotaomicron* MAGs increased after SCI (E to G). All box plots shown display the median and quartiles, with each dot in the box plot representing an individual mouse sample. Five individual mouse samples are used in each group. All relative abundances shown here are represented as reads per kilobase per million mapped reads (RPKM; see Materials and Methods) of differentially abundant species-level MAGs. \*\*,  $P < 0.01$ ; \*,  $P < 0.05$  (by Wilcoxon rank sum test with an FDR of  $< 0.05$ ).

*L. johnsonii* MAG revealed that it harbors the gene encoding the anti-inflammatory enzyme lactocepin (Fig. 4D; Data Set S1, tab 6) but not inulin metabolism genes, such as those coding for fructosyltransferases and fructansucrase (74–77). Since this MAG is only ~85% complete, we cannot rule out that inulin metabolism genes are present in the native population, as others have reported (74–77), even though we did not detect it. Assuming that this MAG is functionally analogous, we hypothesize that after SCI, the dramatic difference in abundance ( $> 8$ -fold) (Fig. 3B) of gut *L. johnsonii* markedly reduces beneficial SCFAs and impairs the immune regulatory properties of the gut microbiome. In support of this hypothesis, we previously reported that postinjury oral supplementation with a probiotic mixture of *Lactobacillus* and *Bifidobacterium* boosted T regulatory cells in the gut-associated lymphoid tissue (GALT) of SCI mice and that these changes were associated with improved locomotor recovery (19). In addition, fecal microbiota transplants restore SCFA levels after SCI and improve recovery (78).

Additionally, of the novel species that decreased, two belonged to the genus *CAG-1031* (family *Muribaculaceae*) and were represented by two high-quality ( $> 90\%$  completeness,  $< 5\%$  contamination) MAGs (Wilcoxon rank sum test,  $P < 0.05$ , FDR  $< 0.05$ ) (Fig. 3C and D). *CAG-1031* spp. decreased significantly with great magnitude ( $> 5$ -fold) in T4 SCI mice, and though they decreased ( $> 4$ -fold) in T10 mice, an outlier caused these changes to be not significant (Fig. 3C and D). Though there are no published *CAG-1031* functions, as a newly classified taxon under the latest GTDB update (69), members of the *Muribaculaceae* are known to synthesize folate and use diverse glycoside hydrolases to degrade complex polysaccharides (79). Indeed, the *CAG-1031* MAGs detected in our samples have the functional capacity to synthesize folate, break down complex polysaccharides, and synthesize vitamin B<sub>6</sub> (Fig. 4D). The significant reduction in such abundant species after SCI suggests marked disruption in the gut microbiome's capacity to metabolize complex carbohydrates and synthesize essential vitamins that cannot be made by mammalian host cells. Given their abundance, strong response, and plausible beneficial roles, we hypothesize that *CAG-1031* spp. are valuable probiotics that, provided they can be grown in culture, might represent a novel probiotic therapy after SCI.

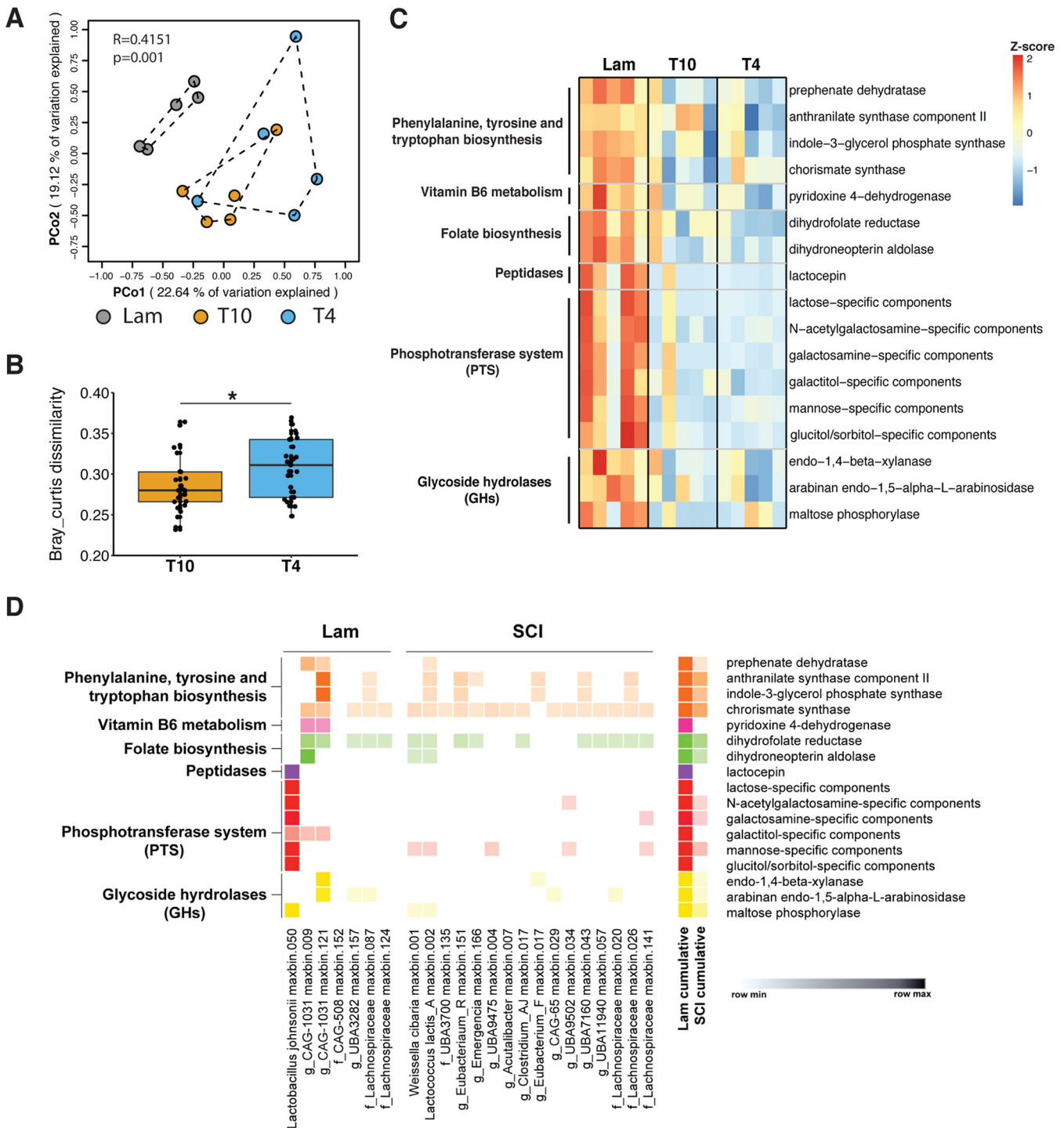


**FIG 4** Predicted metabolic pathways are different between healthy and spinal cord injury animals. (A) Principal-coordinate analysis (PCoA) using Bray-Curtis distances shows that predicted protein clusters are different between the control group Lam and disease groups T4 and T10 (PERMANOVA,  $R=0.4151$ ,  $P \leq 0.001$ ). Each data point indicates an individual mouse sample. (B) Box plot analysis showing the Bray-Curtis dissimilarities of predicted protein clusters for the control groups (Lam) and T4 or T10 SCI groups. Each data point represents one Bray-Curtis dissimilarity comparison between individual samples in each of the other groups (Lam versus T4/T10;  $n=5$  of one group were individually compared to  $n=5$  from another group for a total of 25 comparisons between the Lam and T4 or T10 groups, respectively). (C) Selected functions that are differentially abundant between groups ( $P < 0.05$ , by Wilcoxon rank sum test with a false discovery rate [FDR] of  $< 0.05$  calculated by “fdr” in R used for analysis). (D) MAG-resolved functional analysis for differentially abundant MAGs ( $P < 0.05$  by Wilcoxon rank sum test, FDR  $< 0.05$ ). The x axis shows the names of MAGs which are enriched in the Lam or T10/T4 groups, and the y axis shows the microbial functions from panel C and their predicted pathways. Only the MAGs with at least 80% completeness and less than 10% contamination are displayed here. The mean relative abundances (represented by reads per kilobase per million mapped reads [RPKM]) of KEGG functions of the differentially abundant MAGs were plotted (Morpheus; <https://software.broadinstitute.org/morpheus/>). A relative color scheme was used based on the minimum and maximum values in each row to convert values to colors.



On the other hand, the relative abundances of three previously known bacterial species increased after SCI. *Weissella cibaria* and *Lactococcus lactis\_A* MAGs were significantly enriched only in samples from T4 SCI mice (Wilcoxon rank sum test,  $P < 0.05$ , FDR  $< 0.05$ ) (Fig. 3E and F). Like *L. johnsonii* (above), *W. cibaria* and *Lactococcus lactis\_A* are lactic acid producers (80, 81), and their expansion in the gut of T4 SCI mice may indicate the opportunistic growth of a species that was previously outcompeted by *L. johnsonii* and/or *CAG-1031* spp. In fact, both *W. cibaria* and *Lactococcus lactis\_A* can act as opportunistic pathogens (80, 82), due to virulence factors such as hemolysins (80), which were found in our *W. cibaria* and *Lactococcus lactis\_A* MAGs (Data Set S1, tab 7). *B. thetaiotaomicron* MAG also increased after SCI (Fig. 3G). *B. thetaiotaomicron* is the second most common agent in anaerobic Gram-negative infections in humans (83, 84) and is known to infect immune cells in a sulfatase-dependent manner and express proinflammatory lipooligosaccharides (LOS), which are analogous to the lipopolysaccharides (LPS) found in other Gram-negative bacterial families (85, 86). An analysis of our *B. thetaiotaomicron* MAG predicts that these bacteria carry lipopolysaccharide (LPS), polysaccharide, O-antigen biosynthesis genes, and multiple antibiotic resistance and sulfatase genes (Data Set S1, tab 7). Thus, an increase in *B. thetaiotaomicron* after SCI is expected to increase inflammation locally in the gut and also systemically via translocation.

Collectively, these data suggest that SCI decreases commensal abundances, which may open niches for antagonistic commensals and opportunistic pathogens that can increase inflammation and impair recovery after SCI. However, since most ( $>90\%$ ) of these MAGs represent novel species, the metagenomic approach provides an opportunity to establish baseline hypotheses beyond taxonomy about metabolic versatility—such as the vitamin B<sub>6</sub>, virulence factors, and LPS genes identified and described here—that could contribute to pathological comorbidities common in SCI individuals.

**SCI-induced gut dysbiosis is associated with loss of beneficial microbial functions.** Beyond the MAG-constrained analyses, we next sought to more broadly evaluate functional changes in the microbiome, since functions often vary more than taxonomy, both in human (87) and environmental systems (88). Previous work using 16S sequencing to characterize gut dysbiosis in a rat model of cervical SCI predicted differences in microbial functions between healthy and SCI rats using the PICRUSt algorithm (27). Although tools (i.e., PICRUSt) to infer microbial function from taxonomic profiling can be useful, they do not always correlate with results obtained using metagenomic sequencing (89), and critically, where correlations fail, these are likely to be niche-defining, ecologically relevant genes whose evolutionary histories (i.e., gene flow) are out of sync with slowly evolving ribosomal genes (89). Here, we translated predicted genes from assembled contigs ( $>500$  bp in size) into amino acid sequences and then “organized” sequences into protein clusters. This eliminates bias against analyzing only proteins of known function (see Materials and Methods). As observed before at the taxon level (Fig. 1B), principal coordinate analysis (PCoA) revealed significant clustering of samples from the same group (PERMANOVA,  $R = 0.4151$ ,  $P \leq 0.001$ ) (Fig. 4A), with the largest separation occurring between the Lam and SCI groups. When the between-group Bray-Curtis dissimilarity of each SCI group (T4/T10) was compared with that of healthy controls (Lam), protein cluster changes were exacerbated in mice with high-level T4 SCI (Fig. 4B). Although several metabolic genes were differentially abundant between the T4 and T10 SCI groups (Fig. S4B and Data set S1, tabs 8 and 9), Shannon’s diversity index was not different between the SCI groups (Fig. S4A). These data indicate that SCI-induced disruption of gut microbial composition is accompanied by a corresponding change in microbial function and that these changes are exacerbated in mice with high-level T4 SCI.

To test the hypothesis that SCI impairs beneficial, microbially encoded metabolic functions in the gut, we performed both gene-based abundance comparisons on the whole microbial community (from the assembled contigs) and genome-based metabolic reconstructions (from the recovered MAGs). For gene-based analyses, all predicted functions in Lam controls were compared to those in SCI groups using the

KEGG hierarchy to organize these functions into metabolic modules. Genes that were differentially abundant between the Lam and SCI groups (see Materials and Methods) fell into eight major metabolic pathways—carbohydrate, amino acid, lipid, vitamin, energy, glycan biosynthesis, enzymes involved in metabolism and other metabolisms, including biosynthesis of secondary metabolites, and xenobiotics biodegradation and metabolism (Wilcoxon rank sum test,  $P < 0.05$ , FDR  $< 0.05$ ) (Fig. S4 and Data Set S1, tab 8 and 9). After SCI, especially T4 SCI, we found significant derangement of gut microbial function, including lower abundance of many genes encoding components of the phosphotransferase system (PTS) and glycosyl hydrolases (GHs) (Fig. 4C; Fig. S4B). The PTS system controls sugar uptake by microbes; a reduction in PTS genes can impair microbial sugar utilization and their physiological functions. Many PTS genes, including those that encode the transport proteins specific for maltose, galactose, mannose, and lactose, were significantly reduced after SCI (compared to Lam). Conversely, mannitol PTS genes were significantly increased after T4 SCI (Fig. 4C; Fig. S4B). Utilization of fructose and glucose can decrease the abundance of beneficial commensals (90) and promote inflammation throughout the body (91). Conversely, utilization of lactose and mannose can decrease inflammation (92). Sugar alcohols like mannitol and sorbitol are more abundant in the mouse gut after antibiotic treatment, and enrichment of these sugar alcohols can promote the growth of the pathogen *Clostridium difficile* (93). Microbial GHs can break down indigestible food sources (e.g., fibers), producing neuroactive metabolites like short-chain fatty acids (94). In our study, genes encoding GHs that degrade xylan, arabinan, and maltose were significantly reduced after SCI compared to Lam (Fig. 4C; Fig. S4B).

Other microbial genes involved in regulating the biosynthesis of folate, vitamin B<sub>6</sub>, and amino acids (e.g., tryptophan, phenylalanine, tyrosine) also were reduced by SCI (Fig. 4C; Fig. S4B). In mammals, folate is essential for *de novo* pyrimidine synthesis, a prerequisite for making DNA. Folate also is critical for the maintenance of gastrointestinal health and neurological function (95, 96). In the context of SCI, recent data indicate that folate augments CNS repair and regeneration (97, 98). Vitamin B<sub>6</sub> also plays a significant role in CNS, as it is required for the synthesis of key neurotransmitters, including epinephrine, dopamine, and serotonin (99, 100). Microbial synthesis of amino acids, notably tryptophan, supports gut barrier integrity and stimulates epithelial renewal. Tryptophan synthesized by microbes is converted to 5-hydroxytryptophan (5-HTP) by enterochromaffin cells in the gut and, when further metabolized to serotonin, influences gut motility (101, 102). 5-HTP also enters the circulation, where it can cross the blood-brain barrier and fuel serotonin synthesis in the brain and spinal cord (101–103). Decreased serotonin production has been linked to many disorders, including depression, anxiety, and irritable bowel syndrome (IBS), indicating that loss or a reduction in microbe-dependent tryptophan metabolism after SCI could be an undiagnosed cause or contributor to the higher-than-normal incidence of depression, fatigue, and anxiety in SCI individuals (104–107).

Finally, the microbial gene encoding lactocepin, an anti-inflammatory bacterial protease, was reduced after SCI. Lactocepin selectively degrades inflammatory chemokines, thereby reducing inflammation. Thus, a reduction in lactocepin would favor gut inflammation. In fact, in a murine colitis model, replenishing gut microbes that produce lactocepin effectively reduces gut pathology (108). After SCI, inflammatory cascades are initiated in the gut, and these can impair function of the enteric nervous system, which when combined with loss of normal autonomic tone to the gastrointestinal tract might exacerbate the consequences of a neurogenic bowel (19, 26, 109).

Next, using our *de novo* synthesized microbial reference genomes (MAGs), we mapped the functional changes shown in Fig. 4C (Data Set S1, tabs 9 and 10) to specific microbial species that were enriched significantly in Lam or SCI groups (Fig. 4D; Fig. S3). After these functional changes were mapped to specific MAGs, the mean relative abundance was plotted using a relative color scheme, showing that the cumulative effect of SCI is a reduction in many of these genes in comparison to Lam controls

(Fig. 4D). Many MAGs, in Lam and SCI groups, contain genes controlling functions related to amino acids and secondary metabolite biosynthesis (chorismate synthase, indole-3-glycerol phosphate synthase, and anthranilate synthase component II). The consistency with which these genes were detected in most MAGs is not surprising, given that these genes are essential for building bacterial biomass, antibiotic production, and microbial community communication through quorum sensing (110–112). However, after SCI, some microbial functions were lost, mainly due to a loss or decrease in specific bacterial lineages (Fig. 4D; Data Set S1, tab 10). For example, the reduction in *L. johnsonii* after SCI leads to a decrease in lactocepin, PTS glucitol/sorbitol-specific components, galactitol-specific components, and lactose-specific components. Notably, the enzyme lactocepin is considered to be specific to *Lactobacillus* (108), and the abundance of lactocepin in our *L. johnsonii* MAG constitutes about 61.1% of the total lactocepin in the whole microbial community. In our analysis, lactocepin was also present in the less abundant *ASF356* MAG (Data Set S1, tab 11), revealing another candidate probiotic that could be mixed with *L. johnsonii* and our two novel *CAG-1031* spp. to collectively cover a large spectrum of microbial functions that are markedly reduced in the gut after SCI. Indeed, the consistent reduction in each of these bacterial species in the gut of SCI mice might enhance gut inflammation and reduce the ability of the microbiota to contribute to the metabolism and biosynthesis of key molecules required throughout the body. These results expand upon published data showing predicted functional changes caused by gut dysbiosis in SCI rats (27). Although SCI-induced changes were predicted in carbohydrate metabolism, bile acid biosynthesis, metabolism of cofactors and vitamins, and lipid biosynthesis in both mouse and rat SCI models, the metagenomic sequencing data in the current report provided additional insight. Specifically, we could map specific gene changes to MAGs that were differentially abundant between Lam and SCI groups (Fig. 4D). As a result, it is now possible to develop novel hypotheses about mechanisms ascribed to particular taxa that may be responsible for any observed functional changes. Such MAG-enabled hypotheses are ideal fodder for designing future interventional studies.

Taken together, these functional data support the hypothesis that SCI-induced gut dysbiosis promotes an inflammatory environment in the gut which could adversely affect gut motility and epithelial barrier integrity. This, in turn, has the potential to enhance bacterial translocation and systemic inflammation, exacerbating neuroinflammation and impairing neurological recovery after SCI. Recovery from SCI may be impaired further due to a reduction in the production and release of precursors needed for neurotransmitter synthesis and also vitamins and cofactors needed for optimal neurological function and CNS repair.

**SCI alters the gut virome.** Given the lack of marker genes for viruses (55), we used *de novo* assembly and population-based approaches to characterize the gut virome. These techniques are well established for characterizing viruses in the oceans and soils (53, 54, 113). In total, we recovered 2,675 viruses above 5 kb and 1,028 viral viruses above 10 kb from the bulk metagenomes. Specifically, population- or species-level taxa above 10 kb were discerned by clustering genomes at >95% average nucleotide identity genome-wide, and genus-level taxa were assigned using gene sharing networks. In total, this revealed 1,028 viral populations (approximately species-level taxonomy [54, 114, 115];  $\geq 10$  kb) (see Materials and Methods), of which virtually all ( $n = 1,016$ ; 98.8% of the 1,028) are novel species (Data Set S1, tab 12; see Materials and Methods). Indeed, exhaustive comparisons were made to public databases, including NCBI RefSeq v88 (4,061 complete genomes; >10 kb) (116) and the Human Gut Virome Database (6,360 viral populations; >10 kb) (34), or an additional 502 mouse gut virus genomes were curated (dereplicated into populations) from the IMG/VR database (117) and a published murine viral particle metagenome (118) (see Materials and Methods). Based on these comparisons, these murine gut viral species, which were previously unknown, expand the known murine gut viral sequence space  $\sim 3$ -fold (Data Set S1, tab 13; see Materials and Methods).

At the genus level, gene-sharing network analyses (119) confidently placed 401 of the 1,028 SCI viral populations in the network as part of 163 viral clusters (VCs; equivalent to genus-level characterization). Of these, 89 VCs (containing 219 viral populations) were exclusive to our data set, whereas 74 VCs (containing 182 viral populations) included reference sequences that derive from human gut viruses and/or the NCBI RefSeq database (Data Set S1, tab 14, and Fig. S5A and B). Among these, only 58 murine gut viral populations could be assigned taxonomy (Fig. S5B), within the order *Caudovirales*, and the relative abundance of these phages was higher in the T4 SCI group (Fig. S5C). Previous studies in murine colitis models and human IBD patients also revealed a disease-dependent increase in *Caudovirales* (45, 118). These findings show that many of our murine gut viruses are unique at both the species and genus level and that murine gut viruses clustered more closely with human gut viral genomes than non-gut-derived viruses (Fig. S6A). Together, this is promising for preclinical SCI murine applicability toward human disease.

With this reference data set in-hand, we next assessed the relative abundance of viral populations via nonredundant read mapping. As with the bacterial component of the gut microbiome, principal coordinate analysis (PCoA) of the gut virome (viral contigs  $\geq 5$  kb) revealed marked separation between the Lam and SCI groups (PERMANOVA,  $R=0.3769$ ,  $P \leq 0.002$ ) (Fig. 5A). Moreover, gut viral within-group community dissimilarity was greater in SCI groups (Wilcoxon rank sum test,  $P < 0.05$ , FDR  $< 0.05$ ) (Fig. 5B), and viral species diversity was significantly increased in a spinal level-dependent manner with greater diversity in the T4 SCI group (Wilcoxon rank sum test,  $P < 0.05$ , FDR  $< 0.05$ ) (Fig. 5C). Viral diversity also increases in obesity and inflammatory bowel disease (45, 120, 121), indicating that SCI-induced changes in the gut virome may be associated with an inflammatory disease state. Further analyses of changes in viral population abundances among the groups revealed a relationship between SCI level and the number of viral populations ( $>5$  kb) affected by SCI, as significant changes were noted in 21 and 57 viral populations in T10 and T4 SCI samples, respectively ( $t$  test adjusted, FDR  $P < 0.05$ ) (Fig. 5D; Data Set S1, tab 15).

We next sought to assign infection types (lytic versus temperate) to the fuller data set of 2,675 viruses ( $>5$  kb). To do this, we analyzed the contigs for prophage-bacterium junctions (attachment sites) (122) and signatures (integrase/site-specific recombinase, excisionase, repressor/antirepressor, and *parA/parB*) (123–126) of temperate phages (see Materials and Methods). This suggested that at least 516 contigs ( $\sim 19.3\%$ ) contained such signatures and so might be considered candidate temperate phages; 49 of these were more confidently temperate phages, as they contained identifiable putative attachment sites and integrase genes (Fig. S6B and Data Set S1, tab 16). These findings are similar to previous studies that established that temperate phages constitute about 20 to 50% of phages in the human gut (42, 127, 128). If we restricted these analyses to the 70 viral populations ( $>5$  kb) that were differentially affected by SCI (Fig. 5D and E), 17 were identified as candidate temperate phages, with 3 confident temperate phages containing both identifiable attachment sites and integrases (Data Set S1, tab 17). Prior to these analyses, the effects of SCI on the virome had not been considered. These novel data indicate that SCI alters the gut virome, with the magnitude of effect being more severe after high-level SCI, impacting both temperate and lytic phages.

To develop hypotheses about how SCI-induced virome changes might impact the microbiome, we next sought to link viral contigs to microbial hosts (MAGs) via commonly used *in silico* approaches (similarity to host k-mer signatures [129], prophages [113], tRNAs [118, 130], and CRISPR spacers [130, 131]) (see Materials and Methods). These analyses predicted hosts for 35.5% of the viral contigs (Fig. S7 and Data Set S1, tab 18), which is three times higher than a previous murine gut virome analysis where only reference microbial genome databases were available (118) but on par with findings in soils where cosampled MAGs were also available (113). Using these prediction models, specific phages were significantly altered by SCI (Fig. 6; Fig. S6, Wilcoxon rank

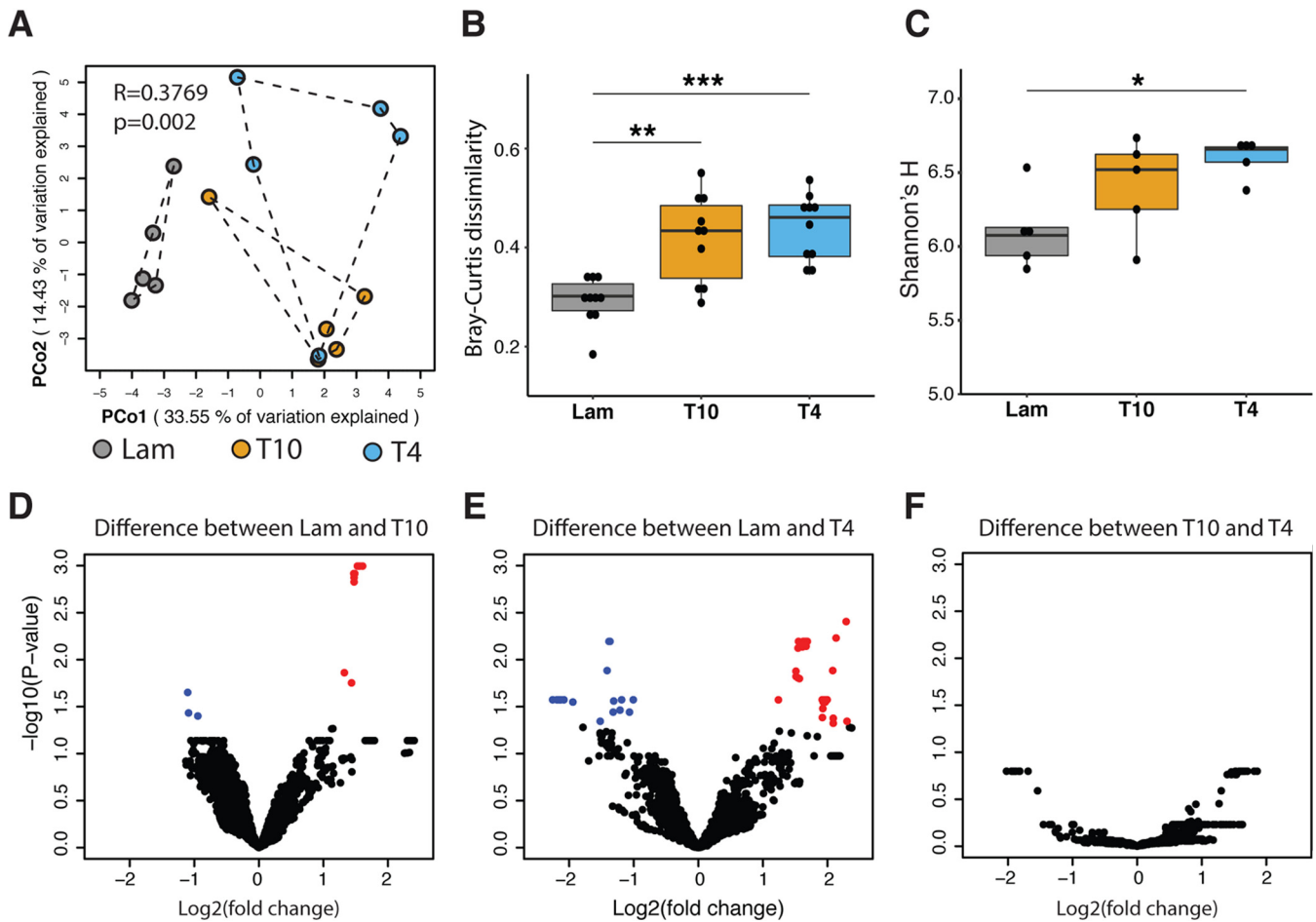


**FIG 5** Viral communities are altered after SCI. (A) Principal-coordinate analysis (PCoA) of Bray-Curtis distances showing that viral communities are different between the Lam, T10, and T4 groups (analysis of similarity [ANOSIM],  $P=0.003$ ). Each data point represents an individual mouse sample ( $n=15$ ). (B) Box plot analysis showing the within-group Bray-Curtis dissimilarities in Lam, T4, and T10 viral communities. A higher score suggests higher dissimilarity of different samples in the same group. \*\*\*,  $P < 0.001$ ; \*\*,  $P < 0.01$  (by Wilcoxon rank sum test with a false discovery rate [FDR] of  $< 0.05$  calculated by “fdr” in R). (C) Box plot analysis showing Shannon's  $H$  of the viral communities between the Lam, T4, and T10 groups. Shannon's  $H$  is an index of diversity, and a higher Shannon's  $H$  suggests higher diversity of viral populations in the communities. All box plots shown display the median and quartiles, with each dot in the box plot representing an individual mouse sample, and each group (Lam, T4, T10) contains five samples. \*,  $P < 0.05$  (by Wilcoxon rank sum test with an FDR of  $< 0.05$ ). (D to F) Volcano plots of  $t$  tests corrected by the Benjamini and Hochberg method for changes to viral population abundances after SCI. An FDR cutoff of 0.05 was used. Data points highlighted in red indicate viral populations that were significantly enriched in T10 or T4 mice, while data points highlighted in blue indicate viral populations that were significantly enriched in the Lam mice.

sum test,  $P < 0.05$ , FDR  $< 0.05$ , and Data Set S1, tab 19). Hierarchical clustering of the differentially abundant phages again revealed 3 distinct clusters (Fig. 6A). Cluster 1 identified phages that were less abundant in both SCI groups compared to Lam controls. Phages in clusters 2 and 3 were more abundant in all SCI samples and T4 SCI samples, respectively, than in Lam controls (Fig. 6A). As with their bacterial hosts (Fig. 3), the relative abundances of phages that infect *Lactobacillus*, *CAG-1031*, and *Turicibacter* were reduced after SCI (Wilcoxon rank sum test,  $P < 0.05$ , FDR  $< 0.05$ ) (Fig. 6B to D; Fig. S6), whereas those predicted to infect *Weissella*, *Lactococcus* (Wilcoxon rank sum test,  $P < 0.05$ , FDR  $< 0.05$ ) (Fig. 6E and F) and class *Clostridia* increased after SCI (Wilcoxon rank sum test,  $P < 0.05$ , FDR  $< 0.05$ ) (Fig. 6G). These data illustrate the value of using cosampled microbial reference genomes (i.e., from the same bulk metagenomes) to make predictions about virus-host interactions. The fact that phage abundance patterns after SCI correspond with changes in microbial host abundance (Fig. 3) indicates that phages may also serve as biomarkers of systemic disease or neurological recovery after SCI and possibly in other disease states.

Though the study of viruses in complex communities and viral ecogenomic approaches are in their infancy, particularly for inferring phage lifestyle (e.g., lytic or

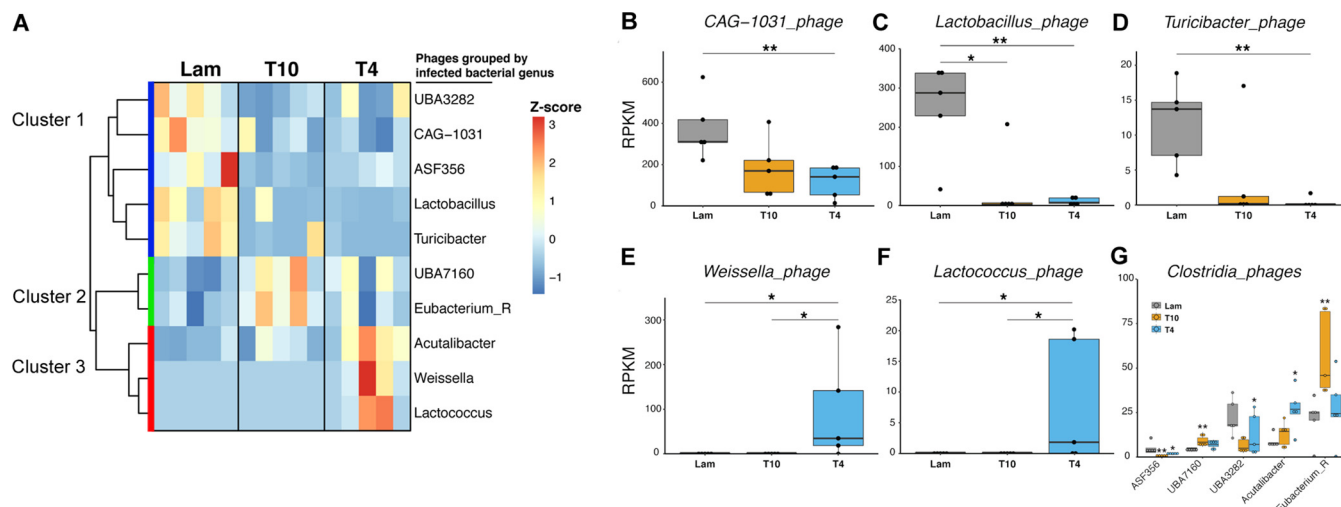


**FIG 6** Viral host prediction reveals that phage abundances vary with their hosts. (A) Hierarchical clustering of these differently abundant phages ( $P < 0.05$  by Wilcoxon rank sum test, FDR  $< 0.05$ ) shows three distinct clusters. (B to D) Box plot analyses of select groups of phages are shown. Phages that were predicted to infect *CAG-1031*, *Lactobacillus*, and *Turicibacter* genera decreased after spinal cord injury. (E to F) Phages that were predicted to infect *Weissella* and *Lactococcus* increased after spinal cord injury. All box plots shown display the median and quartiles, with each dot in the box plot representing an individual mouse sample. Five individual mouse samples were used in each group. (G) Selected genus-specific phages constituting lower taxonomic ranks of the class *Clostridia*. \*\*,  $P < 0.01$ ; \*,  $P < 0.05$  (by Wilcoxon rank sum test). An FDR of  $< 0.05$  calculated by “fdr” in R was used here.

temperate), understanding phage-host dynamics is likely essential for us to reveal any causal roles played by the gut virome in disease (132). Lytic phages metabolically reprogram their bacterial hosts during infection in ways that alter that host’s output into the ecosystem (133) and ultimately kill their hosts to modulate host abundance and diversity through predator-prey dynamics (reviewed in reference 35). Temperate phages integrate themselves into host genomes and can regulate host gene function (reviewed in reference 134) and/or provide their hosts with new functions, like antibiotic resistance, toxin production, and other functions that may promote the virulence of commensals or confer fitness and competitive advantages to the hosts (123, 135). However, stressors, like antibiotics, hydrogen peroxide, and changes in nutrients and pH, which activate the bacterial host’s SOS response, can induce temperate prophages, causing them to become lytic and ultimately kill host cells (123, 136, 137). Dietary fructose and short-chain fatty acids (SCFAs) were shown to induce *Lactobacillus reuteri* temperate phages (138), and bile salts were shown to induce some *Salmonella* temperate phages (139). Gut inflammation can also increase temperate phage induction in mice (140). Thus, a change in gut phage ecology after SCI, due to actions by both temperate and lytic phages, could dramatically influence how individuals respond to dietary changes and repeated regimens of antibiotics or drug therapies. In turn, these changes could have significant implications for recovery of function and the development of various comorbidities after SCI.

**Conclusions.** The gut microbiome has emerged as an essential component of human development, metabolism, and health, and growing evidence from gene marker data for microbes (1–4, 15) and metagenomic data for microbes and viruses (this study) suggest that this is also true for SCI. It is now clear that key probiotic bacterial populations and genes controlling their physiological functions are lost after SCI, suggesting that repopulating the gut with distinct bacterial taxa, such as *Lactobacillus johnsonii* and *CAG-1031* spp., may help to improve a range of functional outcomes after SCI. Also, SCI-induced changes in the gut microbiota may be influenced by corresponding changes in the gut virome, a previously uncharacterized mechanism associated with gut dysbiosis after SCI. These novel phage-host interactions could influence clinical outcomes and also serve as therapeutic targets. For example, the century-old idea of “phage therapy,” whereby bacterial viruses (or phages) are used to selectively target host pathogens, could represent a novel approach to treat bacterial infections, thereby

reducing the need for antibiotics (141), which are variably effective and also harm commensal bacteria. By leveraging the expanding array of microbiome capabilities and resources (142–144) and the partnered viral ecogenomic toolkits for capture (145, 146) and characterization (52–54), it is now possible to establish novel metagenome-enabled hypotheses regarding the effects of SCI on gut microbial ecology and how those changes can functionally influence mammalian physiology.

## MATERIALS AND METHODS

**Animals and spinal cord injury.** All surgical and postoperative care procedures were performed in accordance with the Ohio State University Institutional Animal Care and Use Committee. Fifteen female C57BL/6 mice from Jackson Laboratories (Bar Harbor, Maine) were used in this study. To minimize external/environmental effects on the microbiota, we were meticulous in our efforts to establish controlled conditions, as follows. All animals were ordered together and arrived in the same cohort from Jackson Laboratories. To prevent gut microbial cross-contamination due to cohabitation, all mice were singly housed upon arrival at our animal facility and for the duration of the study in a vivarium room that contained no other animals. All mice remained in this same room for the duration of the study. No mice received antibiotics or dietary supplements at any point throughout the study. Quantity of food intake was not measured, but all mice received the same standard rodent chow for the duration of the study. Our data show that the effects of SCI are consistent (only one outlier was noted using multivariate statistics; see Fig. 1B as an example) and robust. Moreover, there are clear spinal level-dependent differences.

Mice were anesthetized with an intraperitoneal cocktail of ketamine (80 mg/kg)-xylazine (10 mg/kg), after which a partial laminectomy was performed at the 4th thoracic spine (T4) or the 10th thoracic spine (T10). To create consistent severe SCI in each mouse, the spinal cord located between the T3 and T4 or T10 and T11 vertebrae was crushed by inserting modified no. 5 Dumont forceps (Fine Science Tools; with a tip of 0.4 to 0.2 mm) 2 mm ventrally into the vertebral column on both sides of the spinal cord and then laterally compressing the spinal cord by bringing the forceps tips together completely, so they are touching for 3 s. This lesion leaves the dura intact but creates a severe lesion with minimal sparing of ascending or descending axons in the white matter (147). Postoperatively, animals were hydrated with 2 ml Ringer's solution (subcutaneous) for 5 days. Bladders were voided manually at least twice daily for the duration of the study. No prophylactic antibiotics were used during or after surgery. Fecal samples were collected 21 days postinjury (dpi). Mice were removed from their home cage and placed into a ventilated, aseptic polystyrene compartment, and fresh fecal samples were collected from each mouse into sterile tubes and immediately frozen in liquid nitrogen. Mice were returned to their home cage after sample collection. In total, five mice received a complete crush at T4, five mice received a complete crush at T10, and five mice did not receive any crush after laminectomy (Lam group). In our previous work (19), we collected serial samples from the same Lam mice and showed that laminectomy alone (control for both anesthesia and surgery) did not cause differences in gut microbiota when analyzed using 16S rRNA gene sequencing.

**Ethics approval and consent to participate.** The Institutional Animal Care and Use Committee of the Office of Responsible Research Practices at The Ohio State University approved all animal protocols. All experiments were performed in accordance with the guidelines and regulations of The Ohio State University and are outlined in the *Guide for the Care and Use of Laboratory Animals* from the National Institutes of Health.

**Metagenomic sequencing, read quality control, and contigs assembly.** Bulk DNA was recovered from the 15 fecal samples separately using a ZymoBIOMICS extraction kit. Metagenomic library preparation and shotgun sequencing were conducted at CosmosID using an IonTorrent Ion S5 next-generation sequencing system. On average, 23.5 million single-end reads were generated per sample (range, 15.2 million to 36.2 million reads), with an average read length of 180 bp. Reads were quality trimmed using *bbduk* (<https://jgi.doe.gov/data-and-tools/bbtools/>) from both ends to remove bases with low-quality scores (*qtrim* = *rl*, *trimq* = 10) and positions with high compositional bias (*ftl* = 10, *ftr* = range from 204 to 229 depending on the sample). Reads shorter than 30 bp (*minlength* = 30), with Ns (*maxns* = 0) or with an average quality below 10 (*maq* = 10) were discarded. Mouse reads were removed from all the samples using *bbmap* (<https://jgi.doe.gov/data-and-tools/bbtools/>) by mapping against the genome of our model mouse strain C57BL/6NJ (downloaded from the NCBI assembly database; GCA\_001632555.1) and removing reads with a minimum identity of 95% (*minid* = 0.95). After quality control, all the clean single-end reads were cross-assembled using SPAdes (v3.11.1) (148) in the "read-error correction and assembling" mode and using the *(-iontorrent)* flag. The full k-mer size list (*-k* 21, 33, 55, 77, 99, 127) was used in the assembly. All bioinformatic analyses were performed within the Ohio Supercomputer Center (149). For a visual overview of the bioinformatic analyses, see Fig. S1A in the supplemental material.

**Read-based estimation of microbial diversity and community structure.** Reads from each sample were piped through SingleM (singlem pipe; <https://github.com/wwood/singlem>) to estimate the abundance of discrete taxa down to the strain level (*Sensu* [150]). Relative abundances of taxa, which were used for all phylum- and genus-level comparisons, were calculated from the mean coverage of 14 single-copy marker genes to avoid copy number variations associated with 16S-based estimates of abundance and to increase taxonomic resolution. Abundances of taxa inferred from the coverage of ribosomal protein L2 (rplB), which is widely used for microbial community analysis (151), were used for principal-coordinate analysis of Bray-Curtis dissimilarity. Within- and between-group Bray-Curtis dissimilarity analyses were performed using *vegan* in R. Principal-coordinate analysis (function *capscale* with no

constraints applied) was carried out on the Bray-Curtis dissimilarity matrix (function `vegdist`; method “bray”) after a  $\log_2$  transformation on the relative abundance matrix. A pseudo count of 1 was added to all the cells before this transformation to avoid negative numbers. The three groups that emerged in the ordination plot were tested using a PERMANOVA test (function “anosim”) and were defined on the plot using function “ordihull.” For a visual overview of the bioinformatic analyses, see Fig. S1B.

**Construction of MAGs, estimation of abundance, and taxonomic classification.** Microbial metagenome-assembled genomes (MAGs) were recovered using the coassembly-optimized tool MaxBin 2.0 (v2.2.4) (152), which depends on the tetranucleotide frequencies of the contigs, a phylogenetic marker gene set, and differential coverage binning. First, all reads from each sample were mapped to the coassembled contigs using Bowtie2 (v2.3.4.1) (148). The number of mapped bases (for average coverage calculation) and reads (for calculation of normalized reads per kilobase per million mapped reads [RPKM]) were counted using BEDTools (v2.23.0) (153) in “mapbamsamples.pl” of SqueezeMeta (May 2018 distribution) (154). The MAGs were then binned by MaxBin 2.0 using each sample’s contigs’ coverage (-abund\_list) and the full marker gene set. CheckM (v1.0.12) (155) was then used to assess the quality (completeness and contamination) of the genome bins using the “lineage\_wf” pipeline, and genome bins were filtered at a completeness of  $\geq 60\%$  and a contamination of  $\leq 10\%$ . dRep (v2.2.3) (156) was used then to dereplicate the MAGs at 97% average nucleotide identity (dRep\_97 -comp 60 -con 10 -sa 0.97). After the dereplication, 112 MAGs were recovered ( $>60\%$  complete,  $<10\%$  contamination), including 70 high-quality MAGs ( $>90\%$  complete,  $<5\%$  contamination) and 35 medium-quality MAGs ( $>70\%$  complete,  $<10\%$  contamination) that were recovered from our 15 samples. After the recovery of the MAGs, GTDB-Tk (v0.1.3) (63) was used to assign taxonomic classifications for the 112 MAGs in the “classify\_wf” mode. In total, 9 MAGs can be confidently resolved into bacterial species. In addition, among the rest of the MAGs, 73 MAGs can be assigned to bacterial genera. The coverm (<https://github.com/woodruff/CoverM>) was conducted for mapping the reads in different samples to the reference genome (MAGs) in “genome” mode and “single” parameter. Data Set S1 describes the characteristics of the dereplicated MAGs and the predicted taxon of each MAG. For a visual overview of the bioinformatic analyses, see Fig. S1B.

#### Identification of viral contigs and establishing viral populations from the bulk metagenomes.

With a high sequencing depth (average of 23.5 million reads/sample compared to  $\sim 5$  to 10 million in more typical gut microbiomes [157]) in the bulk metagenomes, we were able to identify putative viral contigs, including a mix of actively infecting lytic viruses and prophages, from the bulk metagenomes following assembly. An ensemble approach was used where, first, all contigs were analyzed using VirSorter (v1.0.5) (158), DeepVirFinder (v1.0) (159), MARVEL (v0.1) (160), and CAT (<https://github.com/dutilh/CAT>). This approach combines homology-based identification (CAT and VirSorter), sequence composition in deep learning (DeepVirFinder), and genomic features in probabilistic models (VirSorter and MARVEL). VirSorter was used in the “bulk metagenome” mode and with selection of the virome database, while DeepVirFinder was allowed to predict contigs down to 300 bp in length. Next, linear contigs of  $\geq 5$  kb and circular contigs of  $\geq 1.5$  kb that were sorted as VirSorter categories 1 to 6, by a DeepVirFinder score of  $\geq 0.7$  ( $P$  value  $< 0.05$ ), and/or by a MARVEL random forest probability of  $\geq 70\%$  were kept for further investigation. Of these contigs, those that were sorted as VirSorter categories 1, 2, 4, and 5, by a DeepVirFinder score of  $\geq 0.9$ , or by a MARVEL probability of  $\geq 90\%$  were considered viral. For the rest of the kept contigs, they were considered viral only if they were identified by at least two tools, VirSorter (categories 3 or 6), DeepVirFinder (score of  $\geq 0.7$  and  $< 0.9$ ), MARVEL (probability of  $\geq 70\%$  and  $< 90\%$ ), and/or CAT (annotated as viral or  $< 40\%$  of the genes were classified nonviral). In total, 29,143 viral contigs were identified, with 2,675 viral contigs of  $\geq 5$  kb and 1,030 viral contigs of  $\geq 10$  kb. Then, the identified putative viral contigs were clustered into viral populations using ClusterGenomes (v1.1.0; <https://bitbucket.org/MAVERICLab/stampede-clustergenomes/src/master/>) at  $\geq 95\%$  nucleotide identity across  $\geq 80\%$  of the shorter genome length (55). This resulted in 2,658 viral populations of  $\geq 5$  kb and 1,028 viral populations of  $\geq 10$  kb (see Data Set S1, tab 20, for VirSorter, Deep VirFinder, MARVEL, and CAT results). Notably, the number of viral populations of  $\geq 5$  kb recovered from the 15 samples in this study significantly exceeds the global average of 1,581 viral populations per study at the same contig length cutoff (34). ClusterGenomes analysis was also conducted using a combination of our 1,028 viral populations with viral populations ( $> 10$  kb) in public databases, including NCBI RefSeq v88 (116), the Human Gut Virome Database (34), and the murine gut virome from the IMG/VR database (117), and one murine viral particle metagenome (118) to determine the novelty of our viral species. For a visual overview of the bioinformatic analyses, see Fig. S1C.

**Viral taxonomy and virus-host predictions.** Viral genus-level taxonomy was assigned using vConTACT 2.0 (v2-0.9.9) (119) by clustering (-rel-mode BLASTP -pcs-mode MCL -vcs-mode ClusterONE) our 1,028 viral populations ( $> 10$  kb) with both the RefSeq viral genome database (v88) (4,061 complete genomes;  $> 10$  kb) (116) and the Human Gut Virome Database (6,360 viral populations;  $> 10$  kb) (34). The viral populations that can be clustered with a viral genome from RefSeq were likely to be assigned to a known viral taxonomic genus, family, or order classified by the International Committee on Taxonomy of Viruses (ICTV) taxonomy. Data Set S1, tab 14, summarizes the viral clusters using vConTACT 2.0. Four different computational methods were used to predict putative hosts for the viral populations, prophage-BLAST, CRISPR spacer matches, tRNA exact matches, and k-mer-based sequence similarity. For prophage-BLAST, the viral genome nucleotide sequences were compared to the MAGs using BLASTn based on a method described previously (161). To improve prediction accuracy, only hits with 100% identity over 100% of the length of viral contigs were used for further prediction. Only prophage-BLAST predictions that can be identified using PHASTER (162) were considered. For CRISPR linkages, MinCED (v0.2.0; <https://github.com/ctSkennerton/minced>) was used to search for prokaryotic



CRISPR spacers (with a minimum of 2 repeats that a CRISPR must contain) from our set of MAGs. Then, the prokaryotic CRISPR spacers were matched to viral contigs using BLASTn. Only hits with at least 95% identity over the whole spacer length were considered. For tRNA linkages, tRNAscan-SE (v1.23) (163) was conducted to identify tRNAs from viral contigs (using the general model -G) and MAGs (using the bacterial model -B). Then, tRNA secondary structure sequences from viral contigs were compared to those from MAGs using BLASTn. Only hits with 100% identity over 100% of the length, and at least one hit in each MAG that was consistent with prophage-BLAST prediction, were considered. For k-mer frequency linkages, host-virus connections were predicted using WIsH (v1.0) (129). To assign *P* values to individual virus-host predictions, we built a null model using all the sequences in the RefSeq viral genomes database. Only WIsH prediction with a *P* of 0 and the consistent predictions from both WIsH with a *P* of <0.05 and prophage-BLAST were considered. Figure S7 and Data Set S1, tab 18, show the results from viral host prediction using different methods.

**Annotating genes and making protein clusters.** We annotated genes on all of the assembled contigs by first predicting the open reading frames (ORFs) using Prodigal (v2.6.3) (164) in the metagenomic mode (-p) and ignoring any masked non-protein-coding sequences (-m) produced by “barrnap.pl” of SqueezeMeta. Next, the ORFs were annotated using a pipeline described previously (165). Briefly, annotations were conducted by running a combination of reciprocal best blast hit searches against the KEGG (Kyoto Encyclopedia of Genes and Genomes) (166) and UniRef90 (167) databases in tandem with HMM searches against Pfams (168). About half of ORFs can be annotated using KEGG, and KEGG annotations were then used for downstream analyses. MMseqs2 (version 4eb5e14267f64f2fb337995bd824e-f279e04f266) (169) was used for clustering of all the protein sequence (cluster -min-seq-id 0.3 -cov-mode 1 -c 0.7 -e 0.00001), and the abundances of all the proteins within each cluster were summed to represent the total abundance of each unique protein clusters (PCs). In total, 335,087 protein clusters were identified for PCoA analyses.

**Identification of candidate temperate phages.** To infer phage lifestyle, prophage-bacterium junctions (attachment sites) (122) and lysogeny signatures were searched to identify candidate temperate phages. Candidate identifiable prophages were first identified with PHASTER (162), followed by manual inspection of the annotations for the presence of the attL and attR attachment sites (att). Then, lysogeny signatures (123–126), including integrase(s)/site-specific recombinase, excisionase, phage repressor/anti-repressor, and ParA/B genes, were searched by annotating genes of the 2,675 viral genomes (>5 kb) against the KEGG (166) and UniRef90 (167) databases in tandem with HMM searches against Pfams (168). A prophage usually inserts into the host genome by integrases, which mediate site-specific recombination between the phage attachment site (attP) and the bacterial attachment site (attB) (170, 171). This results in an inserted prophage flanked by two hybrid sites (attL and attR), also needed for the reverse reaction (excision of the phage from the chromosome) along with excisionases (170, 171). Thus, a viral contig can be considered a typical prophage region if it has an integrase HMM match and attachment sites (attL and attR). Figure S6A is a clear example of a “confident” temperate phage, with putative “att” sites next to an integrase gene in the noncoding region. A viral contig containing only lysogeny markers is considered a “candidate” temperate phage. Figure S6B and Data Set S1, tabs 16 and 17, summarize the results from PHASTER and lysogeny markers.

**Statistical analyses.** All the statistical analyses were conducted using RStudio. The Wilcoxon rank sum test was conducted using the function “wilcox.test” in R, and “pairwise.wilcox.test” with adjusted method “fd” was used to calculate the false discovery rate (FDR). “edgeR” and “limma” in R were used for differential analysis for viral populations (>5 kb) in different treatments. The “ggplot2” R package was used for box plots and bar plots. The R package “VennDiagram” was used for Venn diagram plotting, and “pheatmap” was used for heat maps.

**Data availability.** Scripts used in this manuscript are available on the Sullivan laboratory bitbucket under SCI (<https://bitbucket.org/MAVERICLab/spinal-cord-injury-ion-torrent-project/src/master/>). Raw reads and processed data are available through CyVerse under iVirus folder, including all assembled contigs, microbial MAGs, and viral populations.

## SUPPLEMENTAL MATERIAL

Supplemental material is available online only.

**DATA SET S1**, XLSX file, 3.7 MB.

**FIG S1**, PDF file, 0.8 MB.

**FIG S2**, PDF file, 0.9 MB.

**FIG S3**, PDF file, 0.5 MB.

**FIG S4**, PDF file, 0.4 MB.

**FIG S5**, PDF file, 2.9 MB.

**FIG S6**, PDF file, 1 MB.

**FIG S7**, PDF file, 0.8 MB.

**FIG S8**, PDF file, 0.5 MB.

## ACKNOWLEDGMENTS

We appreciate the help and support from all members of the Popovich and Sullivan laboratories, especially Zhen Guan, Jodie Hall, Dylan Cronin, Ben Bolduc, Dean Vik, Kia

Adams, Garrett Smith, and Christine Sun, who participated in animal surgery/care, sample collection, data analysis, and story development. Computational support was provided by an award from the Ohio Supercomputer Center (149) to M.B.S.

We declare that we have no competing interests.

This work was funded by a National Institutes of Neurological Disorders and Stroke R35 award (grant no. 1R35NS111582) to P.G.P., The Belford Center for Spinal Cord Injury (P.G.P.), The Ray W. Poppleton Research designated endowment (P.G.P.), a National Institutes of Health Medical Scientist Training Program T32 grant (K.Z.), and a Gordon and Betty Moore Foundation Investigator Award (no. 3790) to M.B.S.

P.G.P. and K.A.K. conceived the project and experimental design. P.G.P., K.A.K., A.A.Z., and M.B.S. developed the data analysis plan and helped with data interpretation and writing of the manuscript. J.D. performed the statistical and community/taxonomic/functional profiling analyses, generated figures, and contributed to the bioinformatic analyses and manuscript writing. K.Z. contributed to data interpretation and helped write the manuscript. A.A.Z. designed and performed the bioinformatic analyses and contributed to data interpretation, figure generation, and manuscript writing. K.A.K. performed the murine spinal cord injuries as well as daily care and sample collection. All authors approved the manuscript in its final form.

## REFERENCES

- Pickard JM, Zeng MY, Caruso R, Núñez G. 2017. Gut microbiota: role in pathogen colonization, immune responses, and inflammatory disease. *Immunol Rev* 279:70–89. <https://doi.org/10.1111/imr.12567>.
- Hayes CL, Dong J, Galipeau HJ, Jury J, McCarville J, Huang X, Wang XY, Naidoo A, Ambazhagan AN, Libertucci J, Sheridan C, Dudeja PK, Bowdish DME, Surette MG, Verdu EF. 2018. Commensal microbiota induces colonic barrier structure and functions that contribute to homeostasis. *Sci Rep* 8:14184. <https://doi.org/10.1038/s41598-018-32366-6>.
- Rowland I, Gibson G, Heinken A, Scott K, Swann J, Thiele I, Tuohy K. 2018. Gut microbiota functions: metabolism of nutrients and other food components. *Eur J Nutr* 57:1–24. <https://doi.org/10.1007/s00394-017-1445-8>.
- Yoshimoto S, Loo TM, Atarashi K, Kanda H, Sato S, Oyadomari S, Iwakura Y, Oshima K, Morita H, Hattori M, Hattori M, Honda K, Ishikawa Y, Hara E, Ohtani N. 2013. Obesity-induced gut microbial metabolite promotes liver cancer through senescence secretome. *Nature* 499:97–101. <https://doi.org/10.1038/nature12347>.
- Kuno T, Hirayama-Kurogi M, Ito S, Ohtsuki S. 2018. Reduction in hepatic secondary bile acids caused by short-term antibiotic-induced dysbiosis decreases mouse serum glucose and triglyceride levels. *Sci Rep* 8:1253. <https://doi.org/10.1038/s41598-018-19545-1>.
- Roediger WE. 1980. Role of anaerobic bacteria in the metabolic welfare of the colonic mucosa in man. *Gut* 21:793–798. <https://doi.org/10.1136/gut.21.9.793>.
- Flint HJ, Scott KP, Duncan SH, Louis P, Forano E. 2012. Microbial degradation of complex carbohydrates in the gut. *Gut Microbes* 3:289–306. <https://doi.org/10.4161/gmic.19897>.
- Erny D, Hrabě de Angelis AL, Jaitin D, Wieghofer P, Staszewski O, David E, Keren-Shaul H, Mhlahkoiiv T, Jakobshagen K, Buch T, Schwierzeck V, Utermöhlen O, Chun E, Garrett WS, McCoy KD, Diefenbach A, Staeheli P, Stecher B, Amit I, Prinz M. 2015. Host microbiota constantly control maturation and function of microglia in the CNS. *Nat Neurosci* 18:965–977. <https://doi.org/10.1038/nn.4030>.
- Benakis C, Brea D, Caballero S, Faraco G, Moore J, Murphy M, Sita G, Racchumi G, Ling L, Pamer EG, Iadecola C, Anrather J. 2016. Commensal microbiota affects ischemic stroke outcome by regulating intestinal  $\gamma\delta$  T cells. *Nat Med* 22:516–523. <https://doi.org/10.1038/nm.4068>.
- Singh V, Roth S, Llovera G, Sadler R, Garzetti D, Stecher B, Dichgans M, Liesch A. 2016. Microbiota dysbiosis controls the neuroinflammatory response after stroke. *J Neurosci* 36:7428–7440. <https://doi.org/10.1523/JNEUROSCI.1114-16.2016>.
- Winek K, Engel O, Koduah P, Heimesaat MM, Fischer A, Bereswill S, Dames C, Kershaw O, Gruber AD, Curato C, Oyama N, Meisel C, Meisel A, Dirnagl U. 2016. Depletion of cultivatable gut microbiota by broad-spectrum antibiotic pretreatment worsens outcome after murine stroke. *Stroke* 47:1354–1363. <https://doi.org/10.1161/STROKEAHA.115.011800>.
- Chu C, Murdock MH, Jing D, Won TH, Chung H, Kressel AM, Tsaava T, Addorisio ME, Putzel GG, Zhou L, Bessman NJ, Yang R, Moriyama S, Parkhurst CN, Li A, Meyer HC, Teng F, Chavan SS, Tracey KJ, Regev A, Schroeder FC, Lee FS, Liston C, Artis D. 2019. The microbiota regulate neuronal function and fear extinction learning. *Nature* 574:543–548. <https://doi.org/10.1038/s41586-019-1644-y>.
- Strandwitz P. 2018. Neurotransmitter modulation by the gut microbiota. *Brain Res* 1693:128–133. <https://doi.org/10.1016/j.brainres.2018.03.015>.
- Kaelberer MM, Buchanan KL, Klein ME, Barth BB, Montoya MM, Shen X, Bohórquez DV. 2018. A gut-brain neural circuit for nutrient sensory transduction. *Science* 361:eaat5236. <https://doi.org/10.1126/science.aat5236>.
- De Vadder F, Kovatcheva-Datchary P, Goncalves D, Vinera J, Zitoun C, Duchamp A, Bäckhed F, Mithieux G. 2014. Microbiota-generated metabolites promote metabolic benefits via gut-brain neural circuits. *Cell* 156:84–96. <https://doi.org/10.1016/j.cell.2013.12.016>.
- Cryan JF, Dinan TG. 2012. Mind-altering microorganisms: the impact of the gut microbiota on brain and behaviour. *Nat Rev Neurosci* 13:701–712. <https://doi.org/10.1038/nrn3346>.
- Kigerl KA, Mostacada K, Popovich PG. 2018. Gut microbiota are disease-modifying factors after traumatic spinal cord injury. *Neurotherapeutics* 15:60–67. <https://doi.org/10.1007/s13311-017-0583-2>.
- Mayer EA. 2011. Gut feelings: the emerging biology of gut-brain communication. *Nat Rev Neurosci* 12:453–466. <https://doi.org/10.1038/nrn3071>.
- Kigerl KA, Hall JC, Wang L, Mo X, Yu Z, Popovich PG. 2016. Gut dysbiosis impairs recovery after spinal cord injury. *J Exp Med* 213:2603–2620. <https://doi.org/10.1084/jem.20151345>.
- Carabotti M, Scirocco A, Maselli MA, Severi C. 2015. The gut-brain axis: interactions between enteric microbiota, central and enteric nervous systems. *Ann Gastroenterol* 28:203–209.
- Kigerl KA, Zane K, Adams K, Sullivan MB, Popovich PG. 2020. The spinal cord-gut-immune axis as a master regulator of health and neurological function after spinal cord injury. *Exp Neurol* 323:113085. <https://doi.org/10.1016/j.expneurol.2019.113085>.
- Gungor B, Adiguzel E, Gursel I, Yilmaz B, Gursel M. 2016. Intestinal microbiota in patients with spinal cord injury. *PLoS One* 11:e0145878. <https://doi.org/10.1371/journal.pone.0145878>.
- Zhang C, Zhang W, Zhang J, Jing Y, Yang M, Du L, Gao F, Gong H, Chen L, Li J, Liu H, Qin C, Jia Y, Qiao J, Wei B, Yu Y, Zhou H, Liu Z, Yang D, Li J. 2018. Gut microbiota dysbiosis in male patients with chronic traumatic complete spinal cord injury. *J Transl Med* 16:353. <https://doi.org/10.1186/s12967-018-1735-9>.
- Zhang C, Jing Y, Zhang W, Zhang J, Yang M, Du L, Jia Y, Chen L, Gong H, Li J, Gao F, Liu H, Qin C, Liu C, Wang Y, Shi W, Zhou H, Liu Z, Yang D. 2019. Dysbiosis of gut microbiota is associated with serum lipid profiles

- in male patients with chronic traumatic cervical spinal cord injury. *Am J Transl Res* 11:4817–4834.
25. Myers SA, Gobejishvili L, Saraswat Ohri S, Garrett Wilson C, Andres KR, Riegler AS, Donde H, Joshi-Barve S, Barve S, Whitemore SR. 2019. Following spinal cord injury, PDE4B drives an acute, local inflammatory response and a chronic, systemic response exacerbated by gut dysbiosis and endotoxemia. *Neurobiol Dis* 124:353–363. <https://doi.org/10.1016/j.nbd.2018.12.008>.
  26. O'Connor G, Jeffrey E, Madorma D, Marcillo A, Abreu MT, Deo SK, Dietrich WD, Daunert S. 2018. Investigation of microbiota alterations and intestinal inflammation post-spinal cord injury in rat model. *J Neurotrauma* 35:2159–2166. <https://doi.org/10.1089/neu.2017.5349>.
  27. Schmidt EKA, Torres-Espina A, Raposo PJF, Madsen KL, Kigerl KA, Popovich PG, Fenrich KK, Fouad K. 2020. Fecal transplant prevents gut dysbiosis and anxiety-like behaviour after spinal cord injury in rats. *PLoS One* 15:e0226128. <https://doi.org/10.1371/journal.pone.0226128>.
  28. Williams R, Murray A. 2015. Prevalence of depression after spinal cord injury: a meta-analysis. *Arch Phys Med Rehabil* 96:133–140. <https://doi.org/10.1016/j.apmr.2014.08.016>.
  29. Post MW, van Leeuwen CM. 2012. Psychosocial issues in spinal cord injury: a review. *Spinal Cord* 50:382–389. <https://doi.org/10.1038/sc.2011.182>.
  30. Migliorini C, Tonge B, Taleporos G. 2008. Spinal cord injury and mental health. *Aust N Z J Psychiatry* 42:309–314. <https://doi.org/10.1080/00048670801886080>.
  31. Fann JR, Bombardier CH, Richards JS, Tate DG, Wilson CS, Temkin N, PRISMS Investigators. 2011. Depression after spinal cord injury: comorbidities, mental health service use, and adequacy of treatment. *Arch Phys Med Rehabil* 92:352–360. <https://doi.org/10.1016/j.apmr.2010.05.016>.
  32. Sutton TDS, Hill C. 2019. Gut bacteriophage: current understanding and challenges. *Front Endocrinol (Lausanne)* 10:784. <https://doi.org/10.3389/fendo.2019.00784>.
  33. Sausset R, Petit MA, Gaboriau-Routhiau V, De Paepe M. 2020. New insights into intestinal phages. *Mucosal Immunol* 13:205–215. <https://doi.org/10.1038/s41385-019-0250-5>.
  34. Gregory AC, Zablocki O, Zayed AA, Howell A, Bolduc B, Sullivan MB. 2020. The gut virome database reveals age-dependent patterns of virome diversity in the human gut. *Cell Host Microbe* 28:724–740.e8. <https://doi.org/10.1016/j.chom.2020.08.003>.
  35. Warwick-Dugdale J, Buchholz HH, Allen MJ, Temperton B. 2019. Host-hijacking and planktonic piracy: how phages command the microbial high seas. *Virology* 16:15. <https://doi.org/10.1186/s12985-019-1120-1>.
  36. de la Cruz F, Davies J. 2000. Horizontal gene transfer and the origin of species: lessons from bacteria. *Trends Microbiol* 8:128–133. [https://doi.org/10.1016/S0966-842X\(00\)01703-0](https://doi.org/10.1016/S0966-842X(00)01703-0).
  37. Abeles SR, Pride DT. 2014. Molecular bases and role of viruses in the human microbiome. *J Mol Biol* 426:3892–3906. <https://doi.org/10.1016/j.jmb.2014.07.002>.
  38. Manrique P, Dills M, Young MJ. 2017. The human gut phage community and its implications for health and disease. *Viruses* 9:141. <https://doi.org/10.3390/v9060141>.
  39. Van Bellegghem JD, Dąbrowska K, Vanechoutte M, Barr JJ, Bollyky PL. 2018. Interactions between bacteriophage, bacteria, and the mammalian immune system. *Viruses* 11:10. <https://doi.org/10.3390/v11010010>.
  40. Nguyen S, Baker K, Padman BS, Patwa R, Dunstan RA, Weston TA, Schlosser K, Bailey B, Lithgow T, Lazarou M, Luque A, Rohwer F, Blumberg RS, Barr JJ. 2017. Bacteriophage transcytosis provides a mechanism to cross epithelial cell layers. *mBio* 8:e01874-17. <https://doi.org/10.1128/mBio.01874-17>.
  41. Barr JJ, Auro R, Furlan M, Whiteson KL, Erb ML, Pogliano J, Stotland A, Wolkowicz R, Cutting AS, Doran KS, Salamon P, Youle M, Rohwer F. 2013. Bacteriophage adhering to mucus provide a non-host-derived immunity. *Proc Natl Acad Sci U S A* 110:10771–10776. <https://doi.org/10.1073/pnas.1305923110>.
  42. Minot S, Sinha R, Chen J, Li H, Keilbaugh SA, Wu GD, Lewis JD, Bushman FD. 2011. The human gut virome: inter-individual variation and dynamic response to diet. *Genome Res* 21:1616–1625. <https://doi.org/10.1101/gr.122705.111>.
  43. Shkoporov AN, Clooney AG, Sutton TDS, Ryan FJ, Daly KM, Nolan JA, McDonnell SA, Khokhlova EV, Draper LA, Forde A, Guerin E, Velayudhan V, Ross RP, Hill C. 2019. The human gut virome is highly diverse, stable, and individual specific. *Cell Host Microbe* 26:527–541.e5. <https://doi.org/10.1016/j.chom.2019.09.009>.
  44. Manrique P, Bolduc B, Walk ST, van der Oost J, de Vos WM, Young MJ. 2016. Healthy human gut phageome. *Proc Natl Acad Sci U S A* 113:10400–10405. <https://doi.org/10.1073/pnas.1601060113>.
  45. Norman JM, Handley SA, Baldrige MT, Droit L, Liu CY, Keller BC, Kambal A, Monaco CL, Zhao G, Fleshner P, Stappenbeck TS, McGovern DP, Keshavarzian A, Mutlu EA, Sauk J, Gevers D, Xavier RJ, Wang D, Parkes M, Virgin HW. 2015. Disease-specific alterations in the enteric virome in inflammatory bowel disease. *Cell* 160:447–460. <https://doi.org/10.1016/j.cell.2015.01.002>.
  46. Zuo T, Lu XJ, Zhang Y, Cheung CP, Lam S, Zhang F, Tang W, Ching JYL, Zhao R, Chan PKS, Sung JYJ, Yu J, Chan FKL, Cao Q, Sheng JQ, Ng SC. 2019. Gut mucosal virome alterations in ulcerative colitis. *Gut* 68:1169–1179. <https://doi.org/10.1136/gutjnl-2018-318131>.
  47. Kang DW, Adams JB, Gregory AC, Borody T, Chittick L, Fasano A, Khoruts A, Geis E, Maldonado J, McDonough-Means S, Pollard EL, Roux S, Sadowsky MJ, Lipson KS, Sullivan MB, Caporaso JG, Krajmalnik-Brown R. 2017. Microbiota transfer therapy alters gut ecosystem and improves gastrointestinal and autism symptoms: an open-label study. *Microbiome* 5:10. <https://doi.org/10.1186/s40168-016-0225-7>.
  48. Nakatsu G, Zhou H, Wu WKK, Wong SH, Coker OO, Dai Z, Li X, Szeto CH, Sugimura N, Lam TY, Yu AC, Wang X, Chen Z, Wong MC, Ng SC, Chan MTV, Chan PKS, Chan FKL, Sung JJ, Yu J. 2018. Alterations in enteric virome are associated with colorectal cancer and survival outcomes. *Gastroenterology* 155:529–541.e5. <https://doi.org/10.1053/j.gastro.2018.04.018>.
  49. Zhao G, Vatanen T, Droit L, Park A, Kostic AD, Poon TW, Vlamakis H, Siljander H, Härkönen T, Hämäläinen AM, Peet A, Tillmann V, Ilonen J, Wang D, Knip M, Xavier RJ, Virgin HW. 2017. Intestinal virome changes precede autoimmunity in type 1 diabetes-susceptible children. *Proc Natl Acad Sci U S A* 114:E6166–E6175. <https://doi.org/10.1073/pnas.1706359114>.
  50. Wook KK, Allen DW, Briese T, Couper JJ, Barry SC, Colman PG, Cotterill AM, Davis EA, Giles LC, Harrison LC, Harris M, Haynes A, Horton JL, Isaacs SR, Jain K, Lipkin WI, Morahan G, Morbey C, Pang ICN, Papenfuss AT, Penno MAS, Sinnott RO, Soldatos G, Thomson RL, Vuillermin PJ, Wentworth JM, Wilkins MR, Rawlinson WD, Craig ME, ENDIA Study Group. 2019. Distinct gut virome profile of pregnant women with type 1 diabetes in the ENDIA study. *Open Forum Infect Dis* 6:ofz025. <https://doi.org/10.1093/ofid/ofz025>.
  51. Ma Y, You X, Mai G, Tokuyasu T, Liu C. 2018. A human gut phage catalog correlates the gut phageome with type 2 diabetes. *Microbiome* 6:24. <https://doi.org/10.1186/s40168-018-0410-y>.
  52. Brum JR, Ignacio-Espinoza JC, Roux S, Douclier G, Acinas SG, Alberti A, Chaffron S, Cruaud C, de Vargas C, Gasol JM, Gorsky G, Gregory AC, Guidi L, Hingamp P, Iudicone D, Not F, Ogata H, Pesant S, Poulos BT, Schwenck SM, Speich S, Dimier C, Kandels-Lewis S, Picheral M, Searson S, Tara Oceans Coordinators, Bork P, Bowler C, Sunagawa S, Wincker P, Karsenti E, Sullivan MB. 2015. Ocean plankton. Patterns and ecological drivers of ocean viral communities. *Science* 348:1261498. <https://doi.org/10.1126/science.1261498>.
  53. Roux S, Brum JR, Dutilh BE, Sunagawa S, Duhaime MB, Loy A, Poulos BT, Solonenko N, Lara E, Poulain J, Pesant S, Kandels-Lewis S, Dimier C, Picheral M, Searson S, Cruaud C, Alberti A, Duarte CM, Gasol JM, Vaqué D, Bork P, Acinas SG, Wincker P, Sullivan MB, Tara Oceans Coordinators. 2016. Ecogenomics and potential biogeochemical impacts of globally abundant ocean viruses. *Nature* 537:689–693. <https://doi.org/10.1038/nature19366>.
  54. Gregory AC, Zayed AA, Conceição-Neto N, Temperton B, Bolduc B, Alberti A, Ardyna M, Arkhipova K, Carmichael M, Cruaud C, Dimier C, Dominguez-Huerta G, Ferland J, Kandels S, Liu Y, Marec C, Pesant S, Picheral M, Pisarev S, Poulain J, Tremblay J, Vik D, Babin M, Bowler C, Culley AI, de Vargas C, Dutilh BE, Iudicone D, Karp-Boss L, Roux S, Sunagawa S, Wincker P, Sullivan MB, Tara Oceans Coordinators. 2019. Marine DNA viral macro- and microdiversity from pole to pole. *Cell* 177:1109–1123.e14. <https://doi.org/10.1016/j.cell.2019.03.040>.
  55. Roux S, Hallam SJ, Woyke T, Sullivan MB. 2015. Viral dark matter and virus-host interactions resolved from publicly available microbial genomes. *Elife* 4:e08490. <https://doi.org/10.7554/eLife.08490>.
  56. Aggarwala V, Liang G, Bushman FD. 2017. Viral communities of the human gut: metagenomic analysis of composition and dynamics. *Mob DNA* 8:12. <https://doi.org/10.1186/s13100-017-0095-y>.
  57. Moreno-Gallego JL, Chou SP, Di Rienzi SC, Goodrich JK, Spector TD, Bell JT, Youngblut ND, Hewson I, Reyes A, Ley RE. 2019. Virome diversity correlates with intestinal microbiome diversity in adult monozygotic twins.

- Cell Host Microbe 25:261–272.e5. <https://doi.org/10.1016/j.chom.2019.01.019>.
58. LeVatte MA, Mabon PJ, Weaver LC, Dekaban GA. 1998. Simultaneous identification of two populations of sympathetic preganglionic neurons using recombinant herpes simplex virus type 1 expressing different reporter genes. *Neuroscience* 82:1253–1267. [https://doi.org/10.1016/S0306-4522\(97\)00314-x](https://doi.org/10.1016/S0306-4522(97)00314-x).
  59. Mabon PJ, LeVatte MA, Dekaban GA, Weaver LC. 1997. Identification of sympathetic preganglionic neurons controlling the small intestine in hamsters using a recombinant herpes simplex virus type-1. *Brain Res* 753:245–250. [https://doi.org/10.1016/S0006-8993\(97\)00010-3](https://doi.org/10.1016/S0006-8993(97)00010-3).
  60. Browning KN, Travagli RA. 2014. Central nervous system control of gastrointestinal motility and secretion and modulation of gastrointestinal functions. *Compr Physiol* 4:1339–1368. <https://doi.org/10.1002/cphy.c130055>.
  61. Furness JB, Costa M, Freeman CG. 1979. Absence of tyrosine hydroxylase activity and dopamine beta-hydroxylase immunoreactivity in intrinsic nerves of the guinea-pig ileum. *Neuroscience* 4:305–310. [https://doi.org/10.1016/0306-4522\(79\)90091-5](https://doi.org/10.1016/0306-4522(79)90091-5).
  62. Větrovský T, Baldrian P. 2013. The variability of the 16S rRNA gene in bacterial genomes and its consequences for bacterial community analyses. *PLoS One* 8:e57923. <https://doi.org/10.1371/journal.pone.0057923>.
  63. Chaumeil PA, Mussig AJ, Hugenholtz P, Parks DH. 2019. GTDB-Tk: a toolkit to classify genomes with the Genome Taxonomy Database. *Bioinformatics* 36:1925–1927. <https://doi.org/10.1093/bioinformatics/btz848>.
  64. Frank DN, St Amand AL, Feldman RA, Boedeker EC, Harpaz N, Pace NR. 2007. Molecular-phylogenetic characterization of microbial community imbalances in human inflammatory bowel diseases. *Proc Natl Acad Sci U S A* 104:13780–13785. <https://doi.org/10.1073/pnas.0706625104>.
  65. Turnbaugh PJ, Hamady M, Yatsunenko T, Cantarel BL, Duncan A, Ley RE, Sogin ML, Jones WJ, Roe BA, Affourtit JP, Egholm M, Henrissat B, Heath AC, Knight R, Gordon JL. 2009. A core gut microbiome in obese and lean twins. *Nature* 457:480–484. <https://doi.org/10.1038/nature07540>.
  66. Chen J, Wright K, Davis JM, Jeraldo P, Marietta EV, Murray J, Nelson H, Matteson EL, Taneja V. 2016. An expansion of rare lineage intestinal microbes characterizes rheumatoid arthritis. *Genome Med* 8:43. <https://doi.org/10.1186/s13073-016-0299-7>.
  67. Fung TC, Vuong HE, Luna CDG, Pronovost GN, Aleksandrova AA, Riley NG, Vavilina A, McGinn J, Rendon T, Forrest LR, Hsiao EY. 2019. Intestinal serotonin and fluoxetine exposure modulate bacterial colonization in the gut. *Nat Microbiol* 4:2064–2073. <https://doi.org/10.1038/s41564-019-0540-4>.
  68. Jing Y, Yang D, Bai F, Zhang C, Qin C, Li D, Wang L, Yang M, Chen Z, Li J. 2019. Melatonin treatment alleviates spinal cord injury-induced gut dysbiosis in mice. *J Neurotrauma* 36:2646–2664. <https://doi.org/10.1089/neu.2018.6012>.
  69. Parks DH, Chuvochina M, Waite DW, Rinke C, Skarshewski A, Chaumeil PA, Hugenholtz P. 2018. A standardized bacterial taxonomy based on genome phylogeny substantially revises the tree of life. *Nat Biotechnol* 36:996–1004. <https://doi.org/10.1038/nbt.4229>.
  70. Bereswill S, Ekmekci U, Escher U, Fiebiger U, Stingl K, Heimesaat MM. 2017. *Lactobacillus johnsonii* ameliorates intestinal, extra-intestinal and systemic pro-inflammatory immune responses following murine *Campylobacter jejuni* infection. *Sci Rep* 7:2138. <https://doi.org/10.1038/s41598-017-02436-2>.
  71. Valladares R, Sankar D, Li N, Williams E, Lai KK, Abdelgeliel AS, Gonzalez CF, Wasserfall CH, Larkin J, Schatz D, Atkinson MA, Triplett EW, Neu J, Lorca GL. 2010. *Lactobacillus johnsonii* N6.2 mitigates the development of type 1 diabetes in BB-DP rats. *PLoS One* 5:e10507. <https://doi.org/10.1371/journal.pone.0010507>.
  72. Furusawa Y, Obata Y, Fukuda S, Endo TA, Nakato G, Takahashi D, Nakanishi Y, Uetake C, Kato K, Kato T, Takahashi M, Fukuda NN, Murakami S, Miyauchi E, Hino S, Atarashi K, Onawa S, Fujimura Y, Lockett T, Clarke JM, Topping DL, Tomita M, Hori S, Ohara O, Morita T, Koseki H, Kikuchi J, Honda K, Hase K, Ohno H. 2013. Commensal microbe-derived butyrate induces the differentiation of colonic regulatory T cells. *Nature* 504:446–450. <https://doi.org/10.1038/nature12721>.
  73. Fujimura KE, Demoor T, Rauch M, Faruqi AA, Jang S, Johnson CC, Boushey HA, Zoratti E, Ownby D, Lukacs NW, Lynch SV. 2014. House dust exposure mediates gut microbiome *Lactobacillus* enrichment and airway immune defense against allergens and virus infection. *Proc Natl Acad Sci U S A* 111:805–810. <https://doi.org/10.1073/pnas.1310750111>.
  74. Anwar MA, Kralj S, Piqué AV, Leemhuis H, van der Maarel MJE, Dijkhuizen L. 2010. Inulin and levan synthesis by probiotic *Lactobacillus gasserii* strains: characterization of three novel fructansucrase enzymes and their fructan products. *Microbiology (Reading)* 156:1264–1274. <https://doi.org/10.1099/mic.0.036616-0>.
  75. Anwar MA, Kralj S, van der Maarel MJ, Dijkhuizen L. 2008. The probiotic *Lactobacillus johnsonii* NCC 533 produces high-molecular-mass inulin from sucrose by using an inulosucrase enzyme. *Appl Environ Microbiol* 74:3426–3433. <https://doi.org/10.1128/AEM.00377-08>.
  76. van de Wiele T, Boon N, Possemiers S, Jacobs H, Verstraete W. 2007. Inulin-type fructans of longer degree of polymerization exert more pronounced in vitro prebiotic effects. *J Appl Microbiol* 102:452–460. <https://doi.org/10.1111/j.1365-2672.2006.03084.x>.
  77. van der Beek CM, Canfora EE, Kip AM, Gorissen SHM, Olde Damink SWM, van Eijk HM, Holst JJ, Blaak EE, Dejong CHC, Lenaerts K. 2018. The prebiotic inulin improves substrate metabolism and promotes short-chain fatty acid production in overweight to obese men. *Metabolism* 87:25–35. <https://doi.org/10.1016/j.metabol.2018.06.009>.
  78. Jing Y, Yu Y, Bai F, Wang L, Yang D, Zhang C, Qin C, Yang M, Zhang D, Zhu Y, Li J, Chen Z. 2021. Effect of fecal microbiota transplantation on neurological restoration in a spinal cord injury mouse model: involvement of brain-gut axis. *Microbiome* 9:59. <https://doi.org/10.1186/s40168-021-01007-y>.
  79. Lagkouvardos I, Lesker TR, Hitch TCA, Gálvez EJC, Smit N, Neuhaus K, Wang J, Baines JF, Abt B, Stecher B, Overmann J, Strowig T, Clavel T. 2019. Sequence and cultivation study of Muribaculaceae reveals novel species, host preference, and functional potential of this yet undescribed family. *Microbiome* 7:28. <https://doi.org/10.1186/s40168-019-0637-2>.
  80. Abriouel H, Lerma LL, Casado Muñoz MC, Montoro BP, Kabisch J, Pichner R, Cho GS, Neve H, Fusco V, Franz CM, Gálvez A, Benomar N. 2015. The controversial nature of the *Weissella* genus: technological and functional aspects versus whole genome analysis-based pathogenic potential for their application in food and health. *Front Microbiol* 6:1197. <https://doi.org/10.3389/fmicb.2015.01197>.
  81. Song AA, In LLA, Lim SHE, Rahim RA. 2017. A review on *Lactococcus lactis*: from food to factory. *Microb Cell Fact* 16:55. <https://doi.org/10.1186/s12934-017-0669-x>.
  82. Chen F, Zhang Z, Chen J. 2018. Infective endocarditis caused by *Lactococcus lactis* subsp. *lactis* and *Pediococcus pentosaceus*: a case report and literature review. *Medicine (Baltimore)* 97:e13658. <https://doi.org/10.1097/MD.00000000000013658>.
  83. Brook I. 2002. Clinical review: bacteremia caused by anaerobic bacteria in children. *Crit Care* 6:205–211. <https://doi.org/10.1186/cc1490>.
  84. Wexler HM. 2007. Bacteroides: the good, the bad, and the nitty-gritty. *Clin Microbiol Rev* 20:593–621. <https://doi.org/10.1128/CMR.00008-07>.
  85. Hickey CA, Kuhn KA, Donermeyer DL, Porter NT, Jin C, Cameron EA, Jung H, Kaiko GE, Wegorzewska M, Malvin NP, Glowacki RW, Hansson GC, Allen PM, Martens EC, Stappenbeck TS. 2015. Colitogenic *Bacteroides thetaiotaomicron* antigens access host immune cells in a sulfatase-dependent manner via outer membrane vesicles. *Cell Host Microbe* 17:672–680. <https://doi.org/10.1016/j.chom.2015.04.002>.
  86. Jacobson AN, Choudhury BP, Fischbach MA. 2018. The biosynthesis of lipooligosaccharide from *Bacteroides thetaiotaomicron*. *mBio* 9:e02289-17. <https://doi.org/10.1128/mBio.02289-17>.
  87. Schloissnig S, Arumugam M, Sunagawa S, Mitreva M, Tap J, Zhu A, Waller A, Mende DR, Kultima JR, Martin J, Kota K, Sunyaev SR, Weinstock GM, Bork P. 2013. Genomic variation landscape of the human gut microbiome. *Nature* 493:45–50. <https://doi.org/10.1038/nature11711>.
  88. Sunagawa S, Coelho LP, Chaffron S, Kultima JR, Labadie K, Salazar G, Djahanschiri B, Zeller G, Mende DR, Alberti A, Cornejo-Castillo FM, Costea PI, Cruaud C, d'Ovidio F, Engelen S, Ferrera I, Gasol JM, Guidi L, Hildebrand F, Kokoszka F, Lepoivre C, Lima-Mendez G, Poulain J, Poulos BT, Royo-Llonch M, Sarmento H, Vieira-Silva S, Dimier C, Picheral M, Searson S, Kandels-Lewis S, Bowler C, de Vargas C, Gorsky G, Grimsley N, Hingamp P, Ludicone D, Jaillon O, Not F, Ogata H, Pesant S, Speich S, Stemmann L, Sullivan MB, Weissenbach J, Wincker P, Karsenti E, Raes J, Acinas SG, Bork P, Tara Oceans Coordinators. 2015. Ocean plankton. Structure and function of the global ocean microbiome. *Science* 348:1261359. <https://doi.org/10.1126/science.1261359>.
  89. Sun S, Jones RB, Fodor AA. 2020. Inference-based accuracy of metagenome prediction tools varies across sample types and functional categories. *Microbiome* 8:46. <https://doi.org/10.1186/s40168-020-00815-y>.
  90. Townsend GE, Han W, Schwalm ND, Raghavan V, Barry NA, Goodman AL, Groisman EA. 2019. Dietary sugar silences a colonization factor in a mammalian gut symbiont. *Proc Natl Acad Sci U S A* 116:233–238. <https://doi.org/10.1073/pnas.1813780115>.

91. Glushakova O, Kosugi T, Roncal C, Mu W, Heinig M, Cirillo P, Sánchez-Lozada LG, Johnson RJ, Nakagawa T. 2008. Fructose induces the inflammatory molecule ICAM-1 in endothelial cells. *J Am Soc Nephrol* 19:1712–1720. <https://doi.org/10.1681/ASN.2007121304>.
92. Sharma V, Smolin J, Nayak J, Ayala JE, Scott DA, Peterson SN, Freeze HH. 2018. Mannose alters gut microbiome, prevents diet-induced obesity, and improves host metabolism. *Cell Rep* 24:3087–3098. <https://doi.org/10.1016/j.celrep.2018.08.064>.
93. Theriot CM, Koenigsnecht MJ, Carlson PE, Hatton GE, Nelson AM, Li B, Huffnagle GB, Li JZ, Young VB. 2014. Antibiotic-induced shifts in the mouse gut microbiome and metabolome increase susceptibility to *Clostridium difficile* infection. *Nat Commun* 5:3114. <https://doi.org/10.1038/ncomms4114>.
94. El Kaoutari A, Armougoum F, Gordon JI, Raoult D, Henrissat B. 2013. The abundance and variety of carbohydrate-active enzymes in the human gut microbiota. *Nat Rev Microbiol* 11:497–504. <https://doi.org/10.1038/nrmicro3050>.
95. Ponziani FR, Cazzato IA, Danese S, Fagioli S, Gionchetti P, Annicchiarico BE, D'Aversa F, Gasbarrini A. 2012. Folate in gastrointestinal health and disease. *Eur Rev Med Pharmacol Sci* 16:376–385.
96. Reynolds E. 2006. Vitamin B12, folic acid, and the nervous system. *Lancet Neurol* 5:949–960. [https://doi.org/10.1016/S1474-4422\(06\)70598-1](https://doi.org/10.1016/S1474-4422(06)70598-1).
97. Iskandar BJ, Rizk E, Meier B, Hariharan N, Bottiglieri T, Finnell RH, Jarrard DF, Banerjee RV, Skene JH, Nelson A, Patel N, Gherasim C, Simon K, Cook TD, Hogan KJ. 2010. Folate regulation of axonal regeneration in the rodent central nervous system through DNA methylation. *J Clin Invest* 120:1603–1616. <https://doi.org/10.1172/JCI40000>.
98. Kang WB, Chen YJ, Lu DY, Yan JZ. 2019. Folic acid contributes to peripheral nerve injury repair by promoting Schwann cell proliferation, migration, and secretion of nerve growth factor. *Neural Regen Res* 14:132–139. <https://doi.org/10.4103/1673-5374.243718>.
99. Ueland PM, Ulvik A, Rios-Avila L, Middtun Ø, Gregory JF. 2015. Direct and functional biomarkers of vitamin B6 status. *Annu Rev Nutr* 35:33–70. <https://doi.org/10.1146/annurev-nutr-071714-034330>.
100. Kennedy DO. 2016. B vitamins and the brain: mechanisms, dose and efficacy—a review. *Nutrients* 8:68. <https://doi.org/10.3390/nu8020068>.
101. Agus A, Planchais J, Sokol H. 2018. Gut microbiota regulation of tryptophan metabolism in health and disease. *Cell Host Microbe* 23:716–724. <https://doi.org/10.1016/j.chom.2018.05.003>.
102. Roager HM, Licht TR. 2018. Microbial tryptophan catabolites in health and disease. *Nat Commun* 9:3294. <https://doi.org/10.1038/s41467-018-05470-4>.
103. Ruddick JP, Evans AK, Nutt DJ, Lightman SL, Rook GA, Lowry CA. 2006. Tryptophan metabolism in the central nervous system: medical implications. *Expert Rev Mol Med* 8:1–27. <https://doi.org/10.1017/S1462399406000068>.
104. Cao Y, Li C, Gregory A, Charlifue S, Krause JS. 2017. Depressive symptomatology after spinal cord injury: a multi-center investigation of multiple racial-ethnic groups. *J Spinal Cord Med* 40:85–92. <https://doi.org/10.1080/10790268.2016.1244314>.
105. Shin JC, Goo HR, Yu SJ, Kim DH, Yoon SY. 2012. Depression and quality of life in patients within the first 6 months after the spinal cord injury. *Ann Rehabil Med* 36:119–125. <https://doi.org/10.5535/arm.2012.36.1.119>.
106. Craig A, Guest R, Tran Y, Middleton J. 2017. Cognitive impairment and mood states after spinal cord injury. *J Neurotrauma* 34:1156–1163. <https://doi.org/10.1089/neu.2016.4632>.
107. Jensen MP, Kuehn CM, Amtmann D, Cardenas DD. 2007. Symptom burden in persons with spinal cord injury. *Arch Phys Med Rehabil* 88:638–645. <https://doi.org/10.1016/j.apmr.2007.02.002>.
108. von Schillde MA, Hörmannspurger G, Weiher M, Alpert CA, Hahne H, Bäuerl C, van Huynegem K, Steidler L, Hrcir T, Pérez-Martínez G, Kuster B, Haller D. 2012. Lactococci secreted by *Lactobacillus* exerts anti-inflammatory effects by selectively degrading proinflammatory chemokines. *Cell Host Microbe* 11:387–396. <https://doi.org/10.1016/j.chom.2012.02.006>.
109. White AR, Holmes GM. 2018. Anatomical and functional changes to the colonic neuromuscular compartment after experimental spinal cord injury. *J Neurotrauma* 35:1079–1090. <https://doi.org/10.1089/neu.2017.5369>.
110. Radwanski ER, Last RL. 1995. Tryptophan biosynthesis and metabolism: biochemical and molecular genetics. *Plant Cell* 7:921–934. <https://doi.org/10.1105/tpc.7.7.921>.
111. Gerth ML, Nigon LV, Patrick WM. 2012. Characterization of the indole-3-glycerol phosphate synthase from *Pseudomonas aeruginosa* PAO1. *Protein J* 31:359–365. <https://doi.org/10.1007/s10930-012-9412-y>.
112. Ma Q, Zhang X, Qu Y. 2018. Biodegradation and biotransformation of indole: advances and perspectives. *Front Microbiol* 9:2625. <https://doi.org/10.3389/fmicb.2018.02625>.
113. Emerson JB, Roux S, Brum JR, Bolduc B, Woodcroft BJ, Jang HB, Singleton CM, Solden LM, Naas AE, Boyd JA, Hodgkins SB, Wilson RM, Trubl G, Li C, Frolking S, Pope PB, Wrighton KC, Crill PM, Chanton JP, Saleska SR, Tyson GW, Rich VI, Sullivan MB. 2018. Host-linked soil viral ecology along a permafrost thaw gradient. *Nat Microbiol* 3:870–880. <https://doi.org/10.1038/s41564-018-0190-y>.
114. Gregory AC, Solonenko SA, Ignacio-Espinoza JC, LaButti K, Copeland A, Sudek S, Maitland A, Chittick L, Dos Santos F, Weitz JS, Worden AZ, Woyke T, Sullivan MB. 2016. Genomic differentiation among wild cyanophages despite widespread horizontal gene transfer. *BMC Genomics* 17:930. <https://doi.org/10.1186/s12864-016-3286-x>.
115. Bobay LM, Ochman H. 2018. Biological species in the viral world. *Proc Natl Acad Sci U S A* 115:6040–6045. <https://doi.org/10.1073/pnas.1717593115>.
116. Brister JR, Ako-Adjei D, Bao Y, Blinkova O. 2015. NCBI viral genomes resource. *Nucleic Acids Res* 43:D571–D577. <https://doi.org/10.1093/nar/gku1207>.
117. Paez-Espino D, Chen IA, Palaniappan K, Ratner A, Chu K, Szeto E, Pillay M, Huang S, Markowitz VM, Nielsen T, Huntemann M, K Reddy TB, Pavlopoulos GA, Sullivan MB, Campbell BJ, Chen F, McMahon K, Hallam SJ, Denef V, Cavicchioli R, Caffrey SM, Streit WR, Webster J, Handley KM, Salekdeh GH, Tsesmetzis N, Setubal JC, Pope PB, Liu WT, Rivers AR, Ivanova NN, Kyrpides NC. 2017. IMG/VR: a database of cultured and uncultured DNA viruses and retroviruses. *Nucleic Acids Res* 45:D457–D465. <https://doi.org/10.1093/nar/gkw1030>.
118. Duerkop BA, Kleiner M, Paez-Espino D, Zhu W, Bushnell B, Hassell B, Winter SE, Kyrpides NC, Hooper LV. 2018. Murine colitis reveals a disease-associated bacteriophage community. *Nat Microbiol* 3:1023–1031. <https://doi.org/10.1038/s41564-018-0210-y>.
119. Bin Jang H, Bolduc B, Zablocki O, Kuhn JH, Roux S, Adriaenssens EM, Brister JR, Kropinski AM, Krupovic M, Lavigne R, Turner D, Sullivan MB. 2019. Taxonomic assignment of uncultivated prokaryotic virus genomes is enabled by gene-sharing networks. *Nat Biotechnol* 37:632–639. <https://doi.org/10.1038/s41587-019-0100-8>.
120. Kim MS, Bae JW. 2016. Spatial disturbances in altered mucosal and luminal gut viromes of diet-induced obese mice. *Environ Microbiol* 18:1498–1510. <https://doi.org/10.1111/1462-2920.13182>.
121. Handley SA, Thackray LB, Zhao G, Presti R, Miller AD, Droit L, Abbink P, Maxfield LF, Kambal A, Duan E, Stanley K, Kramer J, Macri SC, Permar SR, Schmitz JE, Mansfield K, Brenchley JM, Veazey RS, Stappenbeck TS, Wang D, Barouch DH, Virgin HW. 2012. Pathogenic simian immunodeficiency virus infection is associated with expansion of the enteric virome. *Cell* 151:253–266. <https://doi.org/10.1016/j.cell.2012.09.024>.
122. Canchaya C, Proux C, Fournous G, Bruttin A, Brüssow H. 2003. Prophage genomics. *Microbiol Mol Biol Rev* 67:238–276. <https://doi.org/10.1128/mmb.67.2.238-276.2003>.
123. Howard-Varona C, Hargreaves KR, Abedon ST, Sullivan MB. 2017. Lysogeny in nature: mechanisms, impact and ecology of temperate phages. *ISME J* 11:1511–1520. <https://doi.org/10.1038/ismej.2017.16>.
124. Cho EH, Gumpert RL, Gardner JF. 2002. Interactions between integrase and excisionase in the phage lambda excisive nucleoprotein complex. *J Bacteriol* 184:5200–5203. <https://doi.org/10.1128/jb.184.18.5200-5203.2002>.
125. Fogg PC, Rigden DJ, Saunders JR, McCarthy AJ, Allison HE. 2011. Characterization of the relationship between integrase, excisionase and antirepressor activities associated with a superinfecting Shiga toxin encoding bacteriophage. *Nucleic Acids Res* 39:2116–2129. <https://doi.org/10.1093/nar/gkq923>.
126. Atsumi S, Little JW. 2006. Role of the lytic repressor in prophage induction of phage lambda as analyzed by a module-replacement approach. *Proc Natl Acad Sci U S A* 103:4558–4563. <https://doi.org/10.1073/pnas.051117103>.
127. Reyes A, Haynes M, Hanson N, Angly FE, Heath AC, Rohwer F, Gordon JL. 2010. Viruses in the faecal microbiota of monozygotic twins and their mothers. *Nature* 466:334–338. <https://doi.org/10.1038/nature09199>.
128. Stern A, Mick E, Tirosh I, Sagy O, Sorek R. 2012. CRISPR targeting reveals a reservoir of common phages associated with the human gut

- microbiome. *Genome Res* 22:1985–1994. <https://doi.org/10.1101/gr.138297.112>.
129. Galiez C, Siebert M, Enault F, Vincent J, Söding J. 2017. WISH: who is the host? Predicting prokaryotic hosts from metagenomic phage contigs. *Bioinformatics* 33:3113–3114. <https://doi.org/10.1093/bioinformatics/btx383>.
  130. Paez-Espino D, Eloe-Fadrosh EA, Pavlopoulos GA, Thomas AD, Huntemann M, Mikhailova N, Ruben E, Ivanova NN, Kyrpides NC. 2016. Uncovering Earth's virome. *Nature* 536:425–430. <https://doi.org/10.1038/nature19094>.
  131. Edwards RA, McNair K, Faust K, Raes J, Dutilh BE. 2016. Computational approaches to predict bacteriophage-host relationships. *FEMS Microbiol Rev* 40:258–272. <https://doi.org/10.1093/femsre/fuv048>.
  132. Ogilvie LA, Jones BV. 2015. The human gut virome: a multifaceted majority. *Front Microbiol* 6:918. <https://doi.org/10.3389/fmicb.2015.00918>.
  133. Howard-Varona C, Lindback MM, Bastien GE, Solonenko N, Zayed AA, Jang H, Andreopoulos B, Brewer HM, Glavina Del Rio T, Adkins JN, Paul S, Sullivan MB, Duhaime MB. 2020. Phage-specific metabolic reprogramming of virocells. *ISME J* 14:881–895. <https://doi.org/10.1038/s41396-019-0580-z>.
  134. Feiner R, Argov T, Rabinovich L, Sigal N, Borovok I, Herskovits AA. 2015. A new perspective on lysogeny: prophages as active regulatory switches of bacteria. *Nat Rev Microbiol* 13:641–650. <https://doi.org/10.1038/nrmicro3527>.
  135. Fortier LC, Sekulovic O. 2013. Importance of prophages to evolution and virulence of bacterial pathogens. *Virulence* 4:354–365. <https://doi.org/10.4161/viru.24498>.
  136. Samuels AN, Roggiani M, Zhu J, Goulian M, Kohli RM. 2018. The SOS response mediates sustained colonization of the mammalian gut. *Infect Immun* 87:e00711–18. <https://doi.org/10.1128/IAI.00711-18>.
  137. Zhang X, McDaniel AD, Wolf LE, Keusch GT, Waldor MK, Acheson DW. 2000. Quinolone antibiotics induce Shiga toxin-encoding bacteriophages, toxin production, and death in mice. *J Infect Dis* 181:664–670. <https://doi.org/10.1086/315239>.
  138. Oh JH, Alexander LM, Pan M, Schueler KL, Keller MP, Attie AD, Walter J, van Pijkeren JP. 2019. Dietary fructose and microbiota-derived short-chain fatty acids promote bacteriophage production in the gut symbiont *Lactobacillus reuteri*. *Cell Host Microbe* 25:273–284.e6. <https://doi.org/10.1016/j.chom.2018.11.016>.
  139. Hernández SB, Cota I, Ducret A, Aussel L, Casadesús J. 2012. Adaptation and preadaptation of *Salmonella enterica* to bile. *PLoS Genet* 8:e1002459. <https://doi.org/10.1371/journal.pgen.1002459>.
  140. Diard M, Bakkeren E, Cornuault JK, Moor K, Hausmann A, Sellin ME, Loverdo C, Aertsen A, Ackermann M, De Paepe M, Slack E, Hardt WD. 2017. Inflammation boosts bacteriophage transfer between *Salmonella* spp. *Science* 355:1211–1215. <https://doi.org/10.1126/science.aaf8451>.
  141. Gittrich M, Liu Y, Tian F, Crouch A, Jang HB, Du J, Sullivan M. 2020. The ecology of phage resistance: the key to successful phage therapy? *Preprints* 2020:2020050232. <https://doi.org/10.20944/preprints202005.0232.v1>.
  142. Almeida A, Mitchell AL, Boland M, Forster SC, Gloor GB, Tarkowska A, Lawley TD, Finn RD. 2019. A new genomic blueprint of the human gut microbiota. *Nature* 568:499–504. <https://doi.org/10.1038/s41586-019-0965-1>.
  143. Pasolli E, Asnicar F, Manara S, Zolfo M, Karcher N, Armanini F, Beghini F, Manghi P, Tett A, Ghensi P, Collado MC, Rice BL, DuLong C, Morgan XC, Golden CD, Quince C, Huttenhower C, Segata N. 2019. Extensive unexplored human microbiome diversity revealed by over 150,000 genomes from metagenomes spanning age, geography, and lifestyle. *Cell* 176:649–662.e20. <https://doi.org/10.1016/j.cell.2019.01.001>.
  144. Nayfach S, Shi ZJ, Seshadri R, Pollard KS, Kyrpides NC. 2019. New insights from uncultivated genomes of the global human gut microbiome. *Nature* 568:505–510. <https://doi.org/10.1038/s41586-019-1058-x>.
  145. Deng L, Ignacio-Espinoza JC, Gregory AC, Poulos BT, Weitz JS, Hugenholtz P, Sullivan MB. 2014. Viral tagging reveals discrete populations in *Synechococcus* viral genome sequence space. *Nature* 513:242–245. <https://doi.org/10.1038/nature13459>.
  146. Warwick-Dugdale J, Solonenko N, Moore K, Chittick L, Gregory AC, Allen MJ, Sullivan MB, Temperton B. 2019. Long-read viral metagenomics captures abundant and microdiverse viral populations and their niche-defining genomic islands. *PeerJ* 7:e6800. <https://doi.org/10.7717/peerj.6800>.
  147. Faulkner JR, Herrmann JE, Woo MJ, Tansey KE, Doan NB, Sofroniew MV. 2004. Reactive astrocytes protect tissue and preserve function after spinal cord injury. *J Neurosci* 24:2143–2155. <https://doi.org/10.1523/JNEUROSCI.3547-03.2004>.
  148. Langmead B, Salzberg SL. 2012. Fast gapped-read alignment with Bowtie 2. *Nat Methods* 9:357–359. <https://doi.org/10.1038/nmeth.1923>.
  149. Ohio Supercomputer Center. 1987. Ohio Supercomputer Center. Columbus OH: Ohio Supercomputer Center. <http://osc.edu/ark:/19495/f5s1ph73>.
  150. Woodcroft BJ, Singleton CM, Boyd JA, Evans PN, Emerson JB, Zayed AAF, Hoelzle RD, Lamberton TO, McCalley CK, Hodgkins SB, Wilson RM, Purvine SO, Nicora CD, Li C, Frolking S, Chanton JP, Crill PM, Saleska SR, Rich VI, Tyson GW. 2018. Genome-centric view of carbon processing in thawing permafrost. *Nature* 560:49–54. <https://doi.org/10.1038/s41586-018-0338-1>.
  151. Wang Q, Fish JA, Gilman M, Sun Y, Brown CT, Tiedje JM, Cole JR. 2015. Xander: employing a novel method for efficient gene-targeted metagenomic assembly. *Microbiome* 3:32. <https://doi.org/10.1186/s40168-015-0093-6>.
  152. Wu YW, Simmons BA, Singer SW. 2016. MaxBin 2.0: an automated binning algorithm to recover genomes from multiple metagenomic datasets. *Bioinformatics* 32:605–607. <https://doi.org/10.1093/bioinformatics/btv638>.
  153. Quinlan AR, Hall IM. 2010. BEDTools: a flexible suite of utilities for comparing genomic features. *Bioinformatics* 26:841–842. <https://doi.org/10.1093/bioinformatics/btq033>.
  154. Tamames J, Puente-Sánchez F. 2018. SqueezeMeta, a highly portable, fully automatic metagenomic analysis pipeline. *Front Microbiol* 9:3349. <https://doi.org/10.3389/fmicb.2018.03349>.
  155. Parks DH, Imelfort M, Skennerton CT, Hugenholtz P, Tyson GW. 2015. CheckM: assessing the quality of microbial genomes recovered from isolates, single cells, and metagenomes. *Genome Res* 25:1043–1055. <https://doi.org/10.1101/gr.186072.114>.
  156. Olm MR, Brown CT, Brooks B, Banfield JF. 2017. dRep: a tool for fast and accurate genomic comparisons that enables improved genome recovery from metagenomes through de-replication. *ISME J* 11:2864–2868. <https://doi.org/10.1038/ismej.2017.126>.
  157. Sanders JG, Nurk S, Salido RA, Minich J, Xu ZZ, Zhu Q, Martino C, Fedarko M, Arthur TD, Chen F, Boland BS, Humphrey GC, Brennan C, Sanders K, Gaffney J, Jepsen K, Khosroheidari M, Green C, Liyanage M, Dang JW, Phelan VV, Quinn RA, Bankevich A, Chang JT, Rana TM, Conrad DJ, Sandborn WJ, Smarr L, Dorrestein PC, Pevzner PA, Knight R. 2019. Optimizing sequencing protocols for leaderboard metagenomics by combining long and short reads. *Genome Biol* 20:226. <https://doi.org/10.1186/s13059-019-1834-9>.
  158. Roux S, Enault F, Hurwitz BL, Sullivan MB. 2015. VirSorter: mining viral signal from microbial genomic data. *PeerJ* 3:e985. <https://doi.org/10.7717/peerj.985>.
  159. Ren J, Song K, Deng C, Ahlgren NA, Fuhrman JA, Li Y, Xie X, Poplin R, Sun F. 2020. Identifying viruses from metagenomic data using deep learning. *Quant Biol* 8:64–77. <https://doi.org/10.1007/s40484-019-0187-4>.
  160. Amgarten D, Braga LPP, da Silva AM, Setubal JC. 2018. MARVEL, a tool for prediction of bacteriophage sequences in metagenomic bins. *Front Genet* 9:304. <https://doi.org/10.3389/fgene.2018.00304>.
  161. Emerson JB, Thomas BC, Alvarez W, Banfield JF. 2016. Metagenomic analysis of a high carbon dioxide subsurface microbial community populated by chemolithoautotrophs and bacteria and archaea from candidate phyla. *Environ Microbiol* 18:1686–1703. <https://doi.org/10.1111/1462-2920.12817>.
  162. Arndt D, Grant JR, Marcu A, Sajed T, Pon A, Liang Y, Wishart DS. 2016. PHASTER: a better, faster version of the PHAST phage search tool. *Nucleic Acids Res* 44:W16–W21. <https://doi.org/10.1093/nar/gkw387>.
  163. Lowe TM, Eddy SR. 1997. tRNAscan-SE: a program for improved detection of transfer RNA genes in genomic sequence. *Nucleic Acids Res* 25:955–964. <https://doi.org/10.1093/nar/25.5.955>.
  164. Hyatt D, Chen GL, Locascio PF, Land ML, Larimer FW, Hauser LJ. 2010. Prodigal: prokaryotic gene recognition and translation initiation site identification. *BMC Bioinformatics* 11:119. <https://doi.org/10.1186/1471-2105-11-119>.
  165. Wrighton KC, Thomas BC, Sharon I, Miller CS, Castelle CJ, VerBerkmoes NC, Wilkins MJ, Hettich RL, Lipton MS, Williams KH, Long PE, Banfield JF. 2012. Fermentation, hydrogen, and sulfur metabolism in multiple uncultivated bacterial phyla. *Science* 337:1661–1665. <https://doi.org/10.1126/science.1224041>.
  166. Kanehisa M, Goto S. 2000. KEGG: Kyoto encyclopedia of genes and genomes. *Nucleic Acids Res* 28:27–30. <https://doi.org/10.1093/nar/28.1.27>.

167. Suzek BE, Huang H, McGarvey P, Mazumder R, Wu CH. 2007. UniRef: comprehensive and non-redundant UniProt reference clusters. *Bioinformatics* 23:1282–1288. <https://doi.org/10.1093/bioinformatics/btm098>.
168. El-Gebali S, Mistry J, Bateman A, Eddy SR, Luciani A, Potter SC, Qureshi M, Richardson LJ, Salazar GA, Smart A, Sonnhammer ELL, Hirsh L, Paladin L, Piovesan D, Tosatto SCE, Finn RD. 2019. The Pfam protein families database in 2019. *Nucleic Acids Res* 47:D427–D432. <https://doi.org/10.1093/nar/gky995>.
169. Steinegger M, Söding J. 2017. MMseqs2 enables sensitive protein sequence searching for the analysis of massive data sets. *Nat Biotechnol* 35:1026–1028. <https://doi.org/10.1038/nbt.3988>.
170. Groth AC, Calos MP. 2004. Phage integrases: biology and applications. *J Mol Biol* 335:667–678. <https://doi.org/10.1016/j.jmb.2003.09.082>.
171. Fogg PC, Colloms S, Rosser S, Stark M, Smith MC. 2014. New applications for phage integrases. *J Mol Biol* 426:2703–2716. <https://doi.org/10.1016/j.jmb.2014.05.014>.